NUREG/CR-4003
SAND84-1948
RV

Printed December 1984

General Extrapolation Model for an Important Chemical Dose-Rate Effect

K. T. Gillen, R. L. Clough

Prepared by
Sandia National Laboratories
Albuquerque, New Mexico 87185 and Livermore, California 94550
for the United States Department of Energy
under Contract DE-AC04-76DP00789

Prepared for
U. S. NUCLEAR REGULATORY COMMISSION

Available from

GPO Sales Program
Division of Technical Information and Document Control
U.S. Nuclear Regulatory Commission
Washington, D.C. 20555

and

National Technical Information Service
Springfield, Virginia 22161

NUREG/CR-4008
SAND84-1948
RV

GENERAL EXTRAPOLATION MODEL FOR AN IMPORTANT CHEMICAL DOSE-RATE EFFECT

K. T. Gillen and R. L. Clough

December 1984

Sandia National Laboratories
Albuquerque, New Mexico 87185
Operated by
Sandia Corporation
for the
U. S. Department of Energy

Prepared for
Electrical Engineering Instrumentation and Control Branch
Division of Engineering Technology
Office of Nuclear Regulatory Research
U.S. Nuclear Regulatory Commission
Washington, DC 20555
Under Memorandum of Understanding 40-550-75
NRC FIN No. A-1051

ABSTRACT

In order to extrapolate material accelerated aging data, methodologies must be developed based on sufficient understanding of the processes leading to material degradation. One of the most important mechanisms leading to chemical dose-rate effects in polymers involves the breakdown of intermediate hydroperoxide species. A general model for this mechanism is derived based on the underlying chemical steps. The results lead to a general formalism for understanding dose rate and sequential aging effects when hydroperoxide breakdown is important. We apply the model to combined radiation/temperature aging data for a PVC material and show that this data is consistent with the model and that model extrapolations are in excellent agreement with 12-year real-time aging results from an actual nuclear plant. This model and other techniques discussed in this report can aid in the selection of appropriate accelerated aging methods and can also be used to compare and select materials for use in safety-related components. This will result in increased assurance that equipment qualification procedures are adequate.

CONTENTS

LIST OF FIGURES

LIST OF FIGURES (cont'd)

ACKNOWLEDGEMENTS

The authors would like to acknowledge Dean Mitchell, who measured the oxygen permeation rate, Frank Burns, who carried out the gas chromatographic studies, John Nixon of Battelle Columbus Labs, who did the chemiluminescence experiments, and Nancy Dhooge and Carlos Quintana for general technical assistance.

EXECUTIVE SUMMARY

In the presence of air (oxygen), radiation dose-rate effects are often observed. These effects, which must be understood in order to confidently carry out accelerated aging simulations, can be conveniently divided into two distinct types, physical and chemical. Physical dose-rate effects are extremely common during radiation-aging simulations and are caused by diffusion-limited oxidation. At high dose rates, oxidation in a material will use up dissolved oxygen faster than it can be replenished from the surrounding atmosphere by diffusion through the material. This leads to oxidation gradients in the material, with more oxidation near air-exposed surfaces and less in the interior. As the dose rate is lowered, more oxygen-diffusion time per dose is available, so the oxidation will proceed further into the sample; eventually a homogeneously-aged material will result. Since real-time aging occurs at low dose rates where oxidation throughout will usually occur, an important aspect of accelerated aging simulations is to ensure that the accelerated conditions lead to a homogeneously-aged sample. This can be done using various techniques which profile the oxidation across the accelerated-aged samples.

Chemical dose-rate effects occur whenever some chemical step in the kinetics underlying degradation occurs on a time scale comparable to the sample exposure time. In a radiation environment at low to moderate temperature, probably the most common possibility of a chemical dose-rate effect involves the slow breakdown of intermediate hydroperoxide species. This breakdown is expected to take hundreds to thousands of hours at the aging temperatures expected during nuclear power plant operation (~50°C). In order to extrapolate accelerated aging results in the presence of this and other chemical dose-rate mechanisms, models must be developed based on an understanding of the underlying kinetic mechanisms.

As a detailed example of the above approaches toward carrying out accelerated aging extrapolations in the presence of complications caused by both physical and chemical dose-rate effects, we analyze experimental data on a polyvinylchloride (PVC) cable jacketing material. We first separate the aging of this material in combined radiation/thermal/air environments into two regions, each dominated by a different dose-rate mechanism. The first, which is operative at high dose rates, involves diffusion-limited oxidation; this leads to heterogeneously oxidized samples. The second, which is important at low dose rates and enhanced by elevated temperatures, involves the thermally-induced breakdown of intermediate peroxides formed by the radiation. A metallographic polishing technique together with results from oxygen consumption studies are used to determine the range of dose rates and temperatures for which oxygen diffusion-limited heterogeneous degradation is dominant. In

the remaining homogeneous degradation regime, a general kinetic model is derived. It is based on (1) a number of consensus reactions used for oxidation chemistry, (2) unimolecular termination kinetics, and (3) rate-determining hydroperoxide-mediated branching reactions. Experimental evidence for these kinetics are presented for this PVC material. The model, which generally applies to all hydroperoxide-mediated situations, leads to a number of interesting predictions about dose-rate effects. For example, depending upon the ratio of kinetic rate constants, the hydroperoxide concentration will either tend towards a limiting value (Case I), or continue increasing without limit (Case II). For Case I, dose-rate effects are predicted to disappear at very low dose rates, whereas for Case II they should become progressively more important as the dose rate is lowered. Kinetic analysis of sequential (radiation followed by temperature exposures) aging experiments gives an activation energy for the time-temperature component of the degradation mechanism (i.e., peroxide breakdown). This allows a time-temperature-dose rate shifting procedure to be developed. Using this procedure, higher temperature combined environment results can be shifted to a lower reference temperature, thereby extending the lower temperature results to lower (and experimentally inaccessible) dose rates. By applying this procedure to experimental PVC data, evidence in support of the kinetic model is obtained. Further confirmation occurs when the resulting model predictions for the PVC material are shown to be in excellent agreement with 12-year real-time aging results for identical material removed from a nuclear environment.

The kinetic model and the procedures used for separating heterogeneous degradation effects discussed in this report can aid in the selection of appropriate accelerated aging methods. They can also be used to compare and select materials for use in safety-related components. This will result in increased assurance that equipment qualification procedures are adequate.

INTRODUCTION

We have been interested for some time in the use of accelerated aging tests for making predictions of material life expectancy, especially in combined radiation and temperature environments.[1-3] In order to confidently extrapolate accelerated aging data, models must be developed based on sufficient understanding of the processes leading to the material degradation. This can be quite difficult in a combined environment situation, especially in the presence of air (oxygen).[4] In radiation environments, for example, the presence of oxygen during aging can lead to important radiation dose-rate effects, which have been observed for many years.[5-9] Until recently, such dose-rate effects have been ascribed mostly to oxygen diffusion-limited degradation,[10-12] which is a geometric effect but not a true chemical dose-rate mechanism. Mayo, Decker, and co-workers[13-16] did find evidence for chemical dose-rate effects in unstabilized polymers, which they ascribed to chain propagation by radicals which had escaped their cage. When stabilized with an anti-oxidant, cage escape was found to be suppressed and chemical dose-rate effects disappeared.[14] Thus, until recently there was little concern that important chemical dose-rate effects existed in stabilized, commercial polymeric materials. In a recent paper, where we observed strong dose rate and synergistic effects of combined radiation/temperature/air environments for a stabilized polyvinylchloride (PVC) cable jacketing material and a polyethylene insulation material, we presented evidence that one major cause of these effects was a chemical mechanism involving thermally-induced breakdown of intermediate peroxides initially formed by the radiation.[3] Other recent compelling evidence for the existence of chemical dose-rate effects in stabilized polymers [4,17] and unstabilized polymers[4,18,19] has also been presented. This paper represents an attempt to quantitatively understand the very complicated combined radiation-thermal aging responses for the PVC jacketing material. We have formulated a general kinetic model, which can be utilized to explain radiation dose-rate effects, synergistic effects of radiation and temperature, and sequential (radiation followed by thermal exposure) aging behaviors whenever the hydroperoxide breakdown mechanism is important in radiation aging. The PVC data is used to verify the model, and the resulting extrapolated predictions are shown to agree with 12-year real-time aging data for this material. Since the formation and subsequent breakdown of hydroperoxide species is considered to be important for many polymers in other aging environments (e.g., heat), modifications of the model may make it applicable to thermal as well as radiation environments.

EXPERIMENTAL

Materials

The carbon-black-filled PVC jacketing material used in this study was obtained from a commercial cable manufactured by the

General Cable Corporation and is representative of formulations used in a variety of applications.

Radiation Aging

An extensive series of combined radiation-temperature experiments was carried out in a cobalt-60 facility using radiation dose rates ranging from approximately 20 Gy/h to 1 x 10^4 Gy/h (2 Krad/h to 1 Mrad/h) at temperatures up to 110°C. Aging chambers were equipped with a heating capability that could maintain temperatures in the range of 25 to 150°C, regulated to ± 0.3°C. A slow, steady flow (30 cc/min) of air was supplied to the chamber throughout the course of the experiments. A detailed description and schematics of the aging facility have been published elsewhere.[20]

Tensile Measurements

Tensile tests were performed using an Instron Model 1130 Testing Machine equipped with pneumatic grips and having an extensometer clamped to the sample. The 13 mm thick PVC cable jacketing material was cut with a die into rectangular strip tensile samples having a 5.6 mm width. Samples were strained at ambient temperature at 12.7 cm/min; initial jaw separation was 5.1 cm. At each aging condition typically three samples were tensile tested and averaged to obtain the reported values of the tensile properties. Maximum scatter from the reported values averaged about ± 7 percent of the reported value. Tensile elongation and tensile strength values for the unaged PVC material were 300 ± 10 percent and 20 ± 1 MPa, respectively.

Metallographic Polishing Procedure

Qualitative identification of heterogeneous oxidation in samples irradiated in air at various dose rates and temperatures was accomplished by means of a cross-sectional polishing technique which has been described in detail in a previous publication.[21] By this procedure, samples are mounted in an epoxy, polished by standard metallographic techniques, and examined using a microscope. Oxidized and unoxidized regions are visible as bands of different optical reflectivity.

Thermal Aging

Thermal aging was carried out in our thermal aging oven facility, which allows control of both the gaseous environment (air or nitrogen) and the gas flow rate. This facility has been described previously.[20] Long-term temperature stability is ± 0.5°C. For the present experiments, gas flow rates were approximately 30 cc/min for aging chambers of approximately 500 cc volume.

RESULTS AND DISCUSSION

Separation of Heterogeneous and Homogeneous Aging Data

Representative combined-environment tensile data at 43°C and 73 Gy/h is plotted in Figure 1 for the PVC material. The ultimate tensile strength and ultimate tensile elongation are normalized to their initial (unaged) values and plotted versus aging time in the environment. In general, for this and other PVC jacketing materials, the tensile strength first drops to a plateau as seen in Figure 1, then, dependent on aging conditions, often begins increasing at longer times.[22] As described in a previous paper,[22] oxidative scission dominates the earlier stages of the degradation whereas cross linking appears to become dominant beyond the tensile strength minimum. For this reason, we will concentrate our analysis on the regions where oxidative scission is dominant; i.e., where $e/e_o \geq 0.4$.

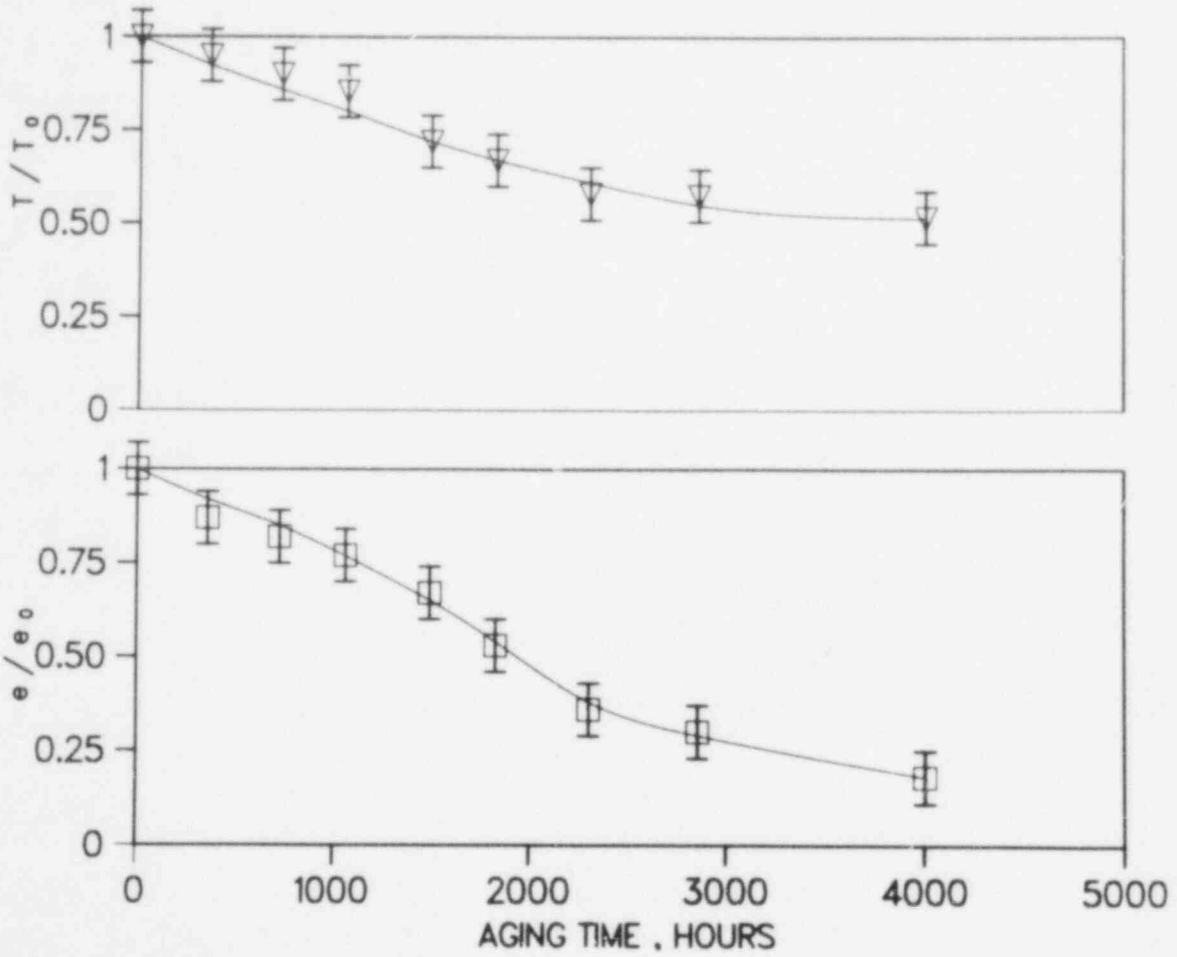

Figure 1. Tensile strength, T, and tensile elongation, e, normalized to their unaged values, T_o, and e_o, plotted versus aging times for PVC aged in air at 43°C and 73 Gy/h.

Figure 2 gives, for example, a plot of the dose to equivalent damage (DED), where damage represents the lowering of the tensile elongation to 40% of original, as a function of the combined environment conditions (dose rate and temperature). Figure 2 shows that upon lowering the radiation dose rate at a given temperature, the DED drops substantially. Moderate increases in temperature also accelerate the degradation. The results, however, are quite complicated. As the dose rate is lowered at 43°C, the curve drops at first indicating dose-rate effects, then appears to level out (small dose-rate effects), and finally begins to drop again, indicating that a second dose-rate-dependent mechanism is becoming important. As the temperature is raised, the plateau region disappears.

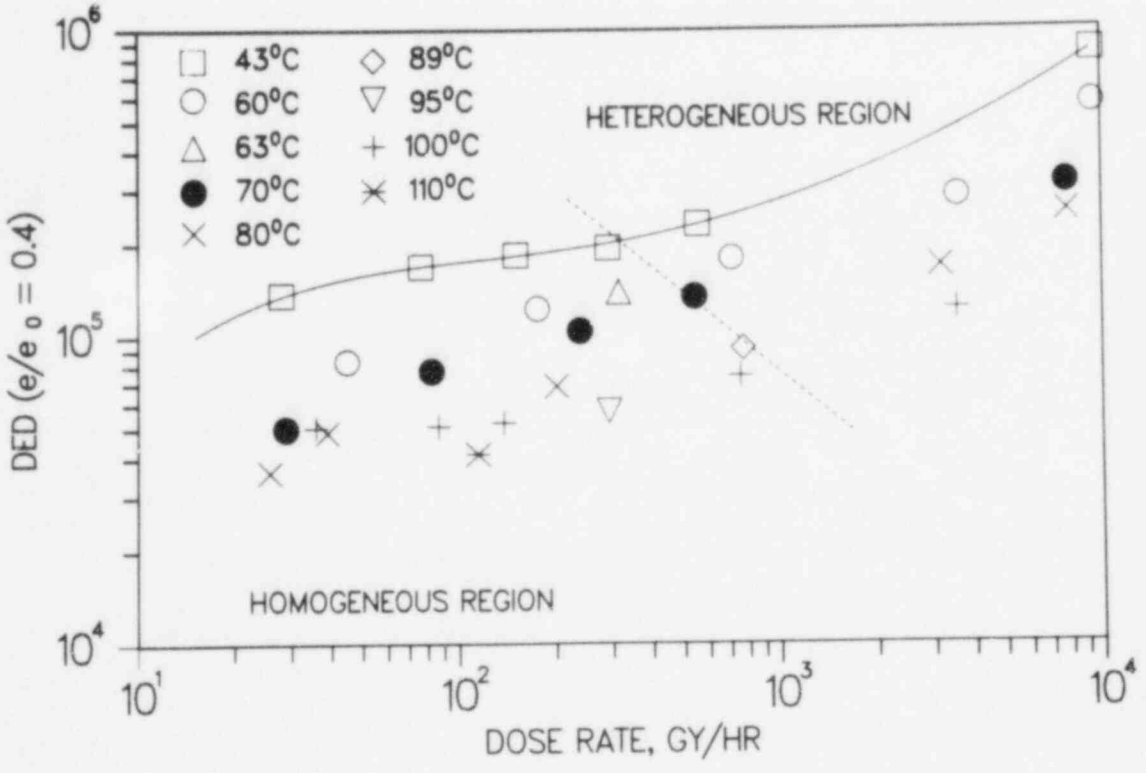

Figure 2. Radiation dose required for the elongation of PVC to decay to 40 percent of its unaged value at various dose rates and temperatures. To highlight the complicated dose-rate effects, a solid curve is drawn through the 43°C data. The dashed curve separates the homogeneous aging region from the heterogeneous aging region.

It has been known for many years that the oxygen-diffusion mechanism can lead to dose-rate effects whenever the rate of oxygen consumption is greater than the rate of oxygen supply from the surrounding atmosphere. An oxygen-starved region results in the interior of the sample. The oxygen-diffusion mechanism, which should eventually disappear at sufficiently low dose rates, is the likely mechanism responsible for the dose-rate effects occurring at the dose rates higher than the plateau region. There are various ways to confirm this hypothesis. Since diffusion-limited degradation leads to a heterogeneously-degraded sample, techniques for profiling degradation across samples can be applied. We recently developed a qualitative profiling technique, metallographic polishing, that can quickly monitor changes in oxidative degradation across small samples. This technique utilizes cross sectioned, polished samples which, when examined under a microscope, reveal oxidized and nonoxidized areas of the sample as bands of different reflectivity.[21]

Figure 3 shows photos of the appearance of typical structure for the PVC material. When oxygen-diffusion-limited degradation is important, a concentric banded structure occurs, with the bands adjacent to the air-exposed surfaces representing the oxidized regions. For a given PVC sample, the thickness of the oxidation band is approximately constant, allowing estimates of the oxidation bandwidths by use of a microscope equipped with a filar eyepiece. Bandwidth results are summarized in Table I, together with the approximate percentage of the sample which was oxidized using an overall sample thickness of 1.24 mm. The results for 9.3×10^3 Gy/h at 43°C, and for 3.56×10^3 Gy/h at 60°C confirm the expectation that important oxygen-diffusion-limited effects occur at the highest dose rates studied. At 80°C and 200 Gy/h there is no evidence of heterogeneous effects. At 293 Gy/h and 43°C the data represent the approximate point where the 43°C dose-rate data first reach the plateau region in Figure 2: the results indicate that oxidation occurs through most but not all of the material. Thus, the polishing results indicate that oxygen-diffusion effects are very important above the 43°C plateau region of Figure 2 and that the oxidation is becoming reasonably homogeneous as the dose rate is lowered through this region.

Although the polishing technique can easily distinguish between regions of heavy and light (or nonexistent) oxidation, it is less useful for distinguishing moderately inhomogeneous oxidation, and cannot be used to quantitatively pinpoint when homogeneous oxidation conditions are reached. More quantitative evidence of where diffusion effects become insignificant can be derived from measurements of the oxygen permeation rate, P_{ox}, and the oxygen consumption rate, Φ. Cunliffe and Davis calculated oxidation profile shapes for material sheets of thickness, L, exposed on both sides to an oxygen partial pressure, p.[23] Although the profile shapes depend on the detailed

Figure 3. Photographs showing appearance of oxidation bands for metallographically polished cross-sectioned PVC sample. Approximate magnifications are 12X for top photo and 30X for bottom photo. Sample was aged to 9.3 x 10^5 Gy at 60°C and 3560 Gy/h.

Table I.

Metallographic Polishing Results for PVC

Dose Rate Gy/h	Temp °C	Dose Gy	Oxidation Bandwidth mm	% Oxidized
9300	43	2.2×10^5	0.138	22
		4.8×10^5	0.160	26
3560	60	3.4×10^5	0.375	61
		9.3×10^5	0.270	43
293	43	2.5×10^5	Total	100
		3.4×10^5	0.540	87
202	80	3.0×10^5	Total	100

oxidation kinetics for a given material, the oxygen consumption rate can be used to estimate the conditions under which homogeneous oxidation occurs. For aging at a dose rate, I, "homogeneous" aging occurs if

$$\frac{I\phi L^2}{8p\ P_{ox}} < \frac{1}{C} \qquad (1)$$

where C is a constant which depends on both the detailed kinetics and the definition of "homogeneous." If we integrate the amount of oxidation across the sample and define "homogeneous" as the conditions under which the integrated oxidation reaches 90% of what completely uniform oxidation would give, C will equal approximately 1. For 95% oxidation, C will be approximately 2.

Measuring the oxygen consumption rate at 43°C for PVC presents some difficulty. Since the consumption rate is needed in the absence of the dose-rate mechanism occurring at dose rates lower than the plateau region, the consumption experiment must be done at dose rates well above this drop-off region. At the same time, oxygen-diffusion effects must be eliminated. For these reasons we dissolved the PVC material in THF and evaporated the solvent to produce sheet material of thickness no greater than 0.2 mm. Two lots of this material were irradiated at 43°C in closed containers which contained oxygen at 590 mm initial pressure. Dose rates used were 810 Gy/h and 480 Gy/h. The high oxygen pressures coupled with the thin samples eliminated

concerns about diffusion effects. After exposures of 8×10^4 Gy, the oxygen consumption was obtained from gas chromatographic estimates of the oxygen pressure remaining in the tubes. The results were that ϕ equals 9.8×10^{-10} moles/Gy/g at both 480 and 810 Gy/h; this implies that neither diffusion nor other dose-rate effect mechanisms are important in these measurements, since both would lead to higher oxygen consumption at the lower dose rate. These results could be affected by the evaporation of solvent from the dissolved material since this procedure may yield a nonhomogeneous material, e.g., heavier components such as clay fillers may settle to the bottom. Results on our actual cable materials were found to be in reasonable agreement with the results from solvent evaporated materials. For instance, at 43°C and 74 Gy/h, ϕ is 11.9×10^{-10} moles/Gy/g but this result may be slightly influenced by the dose-rate mechanism entering at low dose rates. Literature values[24] for oxygen consumption of plasticized PVC are also in accord with our results; thus, we will estimate ϕ to be $11 \pm 3 \times 10^{-10}$ moles/Gy/g. Using this value of ϕ together with the 43°C oxygen permeation rate of 8.9×10^{10} cc/sec cm-cm Hg measured in our laboratory, we can use Equation (1) to calculate that a 90% oxidized sample ($C \sim 1$) should occur at a dose rate of approximately 600 Gy/h and that a 95% oxidized sample ($C \sim 2$) corresponds to ~ 300 Gy/h. This conclusion is consistent with the polishing results discussed earlier and again indicates that heterogeneous oxygen-diffusion effects are responsible for the dose-rate effects above the plateau region at 43°C.

We can use the above results together with temperature dependencies of the oxygen permeation and consumption rates to divide the combined-environment data of Figure 2 into heterogeneous and homogeneous aging regions. The dividing line is, of course, not exact and depends on one's definition of homogeneous. For the remainder of this paper we will be concerned with the homogeneous aging regime where true chemical dose-rate effects become important.

Isothermal Kinetic Model Development

In the homogeneous region we model the kinetics with the following set of chemical reactions:

Initiation

$$\text{Polymer} \xrightarrow{k_I I} R\cdot \qquad (2)$$

Propagation

$$R\cdot + O_2 \xrightarrow{k_1'} RO_2\cdot \qquad (3)$$

$$RO_2\cdot + RH \xrightarrow{k_2'} ROOH + R\cdot \qquad (4)$$

$$RO_2\cdot \xrightarrow{k_3} R\cdot + P_{int} \qquad (5)$$

Branching

$$ROOH \xrightarrow{k_4} RO\cdot + \cdot OH \qquad (6)$$

$$RO\cdot + RH \xrightarrow{k_5'} ROH + R\cdot \qquad (7)$$

$$\cdot OH + RH \xrightarrow{k_6'} HOH + R\cdot \qquad (8)$$

Termination

$$RO_2\cdot \xrightarrow{k_7} P_{term} \qquad (9)$$

Initiation with a dose rate, I, creates free radicals. In the presence of oxygen, these rapidly react to give peroxy radicals ($RO_2\bullet$). The peroxy radicals can either propagate the degradation leading to hydroperoxide (ROOH) and/or internal products, P_{int}, plus a propagating free radical, or terminate leading to termination products. These are all consensus oxidation reactions developed many years ago in studies of oxidation in organic liquids and for polymers in solution. The termination step in our calculations is, however, chosen as unimolecular instead of the bimolecular termination ($RO_2\bullet + RO_2\bullet \rightarrow P_{term}$) found in most liquid and solution studies. In other words, we assume that the rate of termination depends upon the first power of the concentration of $RO_2\bullet$, rather than the second power. Mayo and co-workers[13-16] did find evidence of some bimolecular termination in certain pure polymers at moderate dose rates

(300 to 1200 Gy/h), but evidence for bimolecular kinetics could not be found in the presence of antioxidant.[14] Arakawa and co-workers[18] postulated (without direct evidence) that the dose-rate effects which they observed for a number of unstabilized materials were due to a combination of unimolecular and bimolecular termination kinetics with the former becoming more important as the dose rate was lowered.

We feel that conditions of very low dose rates (which we are attempting to simulate), coupled with the antioxidants present in the commercial materials, favors unimolecular termination kinetics. Termination of peroxy radicals by antioxidant can be pseudo first order if the antioxidant is present in high enough concentration such that it can be considered constant during degradation and therefore be included in the rate constant. Also, for solid polymers it would be expected that the "cage" effect should be very pronounced due to the extremely limited diffusional motions of the polymer molecules. The resultant expectation is that for chain termination which occurs by radical-radical reaction, a large proportion of the terminating radical pairs are geminate--i.e., their origin could be traced to a radical pair which was originally formed from the same bond-breaking event. Furthermore, of the portion of radicals which terminate with nongeminate radical partners, a large fraction are expected to react with radicals which originated from the same localized "track" or "spur" consisting of multiple pairs of radicals created by a single γ-ray as it impacts the material. For radical-radical recombination involving pairs either of geminate origin or of a common "track" origin, the chemical reaction is bimolecular, but the resulting kinetics will be unimolecular. Bimolecular termination kinetics are obtained only when peroxy radicals from different gamma tracks react with each other. It therefore seems clear why unimolecular termination kinetics must be favored at low enough dose rates and why the presence of antioxidants will hasten the transition to these kinetics.

Even at the moderate dose rates which apply to Figure 2, we will offer experimental evidence for the dominance of unimolecular kinetic termination. If the kinetics are steady state analyzed using a bimolecular termination step, the rate of formation of chain termination products will be linear with dose rate, but the rate of internal product and ROOH production will be proportional to $I^{1/2}$ whereas the oxygen consumption rate will involve a combination of a first order and a half order term. For unimolecular termination, all rates will be linear with I (no dose-rate effects). If internal products are important to tensile properties, unimolecular termination must dominate in the plateau region (no dose-rate effects) of Figure 2. The oxygen consumption results for solvent-evaporated material (in the absence of the dose-rate mechanism at low dose rates) are also independent of dose rate, again implying domination by

unimolecular kinetics. We will show below that the production of ROOH is also linear with dose rate in the plateau region. We therefore conclude that unimolecular termination kinetics hold for our PVC material. Since the unimolecular kinetic scheme confirmed above leads to production of products linear with dose rate, we need additional reactions to explain the enhanced degradation rate (per Gy) observed in Figure 2 as the dose rate is lowered and/or the temperature is raised.

In an earlier paper[3] we presented evidence that these effects are due to the breakdown of ROOH species by reaction schemes such as the branching reactions shown in Equations (6)-(8). These reactions lead to more free radicals to participate in the propagation reactions shown earlier. It is known that hydroperoxides are thermally unstable and will break down at elevated temperatures leading to such branching reactions. The breakdown must, therefore, also occur at lower temperatures but over much longer time periods. Since our aging experiments at intermediate dose rates last up to many thousands of hours, there is sufficient time for significant ROOH breakdown to occur at the moderate temperatures experimentally employed.

Sequential experiments (radiation aging followed by oven aging) in air and nitrogen environments were especially useful in confirming this hypothesis. For example, PVC was given 8×10^4 Gy dose in air under conditions where only minimal ROOH breakdown would be expected (40 Gy/h and 22°C). This exposure created hydroperoxides, and led to a lowering in tensile elongation to 80 percent of unaged. Samples not tensile tested after irradiation were divided into two lots, which were aged for 83 days at 80°C in air and nitrogen, respectively, after which their tensile elongations were determined to be 32 percent (air) and 83 percent (nitrogen) of unaged. The large drop during air oven aging was interpreted as coming from the branching reactions shown above. In the nitrogen oven-aging, no further propagation was possible, so little change occurred in tensile properties. To confirm the importance of hydroperoxide breakdown, another group of samples was irradiated to 9.2×10^4 Gy under identical radiation-aging conditions, after which the elongation was found to have dropped to 74 percent of the unaged value. Half of the samples not tensile tested were 80°C oven aged in air for 25 days, resulting in an elongation equal to 38 percent of unaged. The other half were treated with PH_3 gas (a peroxide scavenger) and then oven aged in air under identical conditions. The tensile elongation remained constant, further confirming the ROOH breakdown mechanism.

In the absence both of important diffusion effects and important ROOH breakdown (i.e., in the plateau region for PVC at 43°C), another type of sequential aging experiment can be used to confirm the existence of unimolecular termination kinetics. One group of PVC samples was given 6.3×10^4 Gy in air at 43°C

and 76 Gy/h while a second group was given the same dose in air at 43°C and 148 Gy/h. If unimolecular termination is operative, the ROOH concentration of both groups of samples should be identical, if bimolecular termination is dominant, the samples aged at the lower dose rate should have a 40 percent higher ROOH concentration, since $(148/76)^{0.5} = 1.40$. The two groups of irradiated samples were placed in a 90°C air-circulating oven in order to break down the hydroperoxides, leading to further material damage which was monitored by following tensile properties. The resulting degradation behaviors, shown in Figure 4, were almost identical, implying almost identical ROOH concentrations after the radiation aging part of the sequence. This is further evidence in support of the dominance of unimolecular termination.

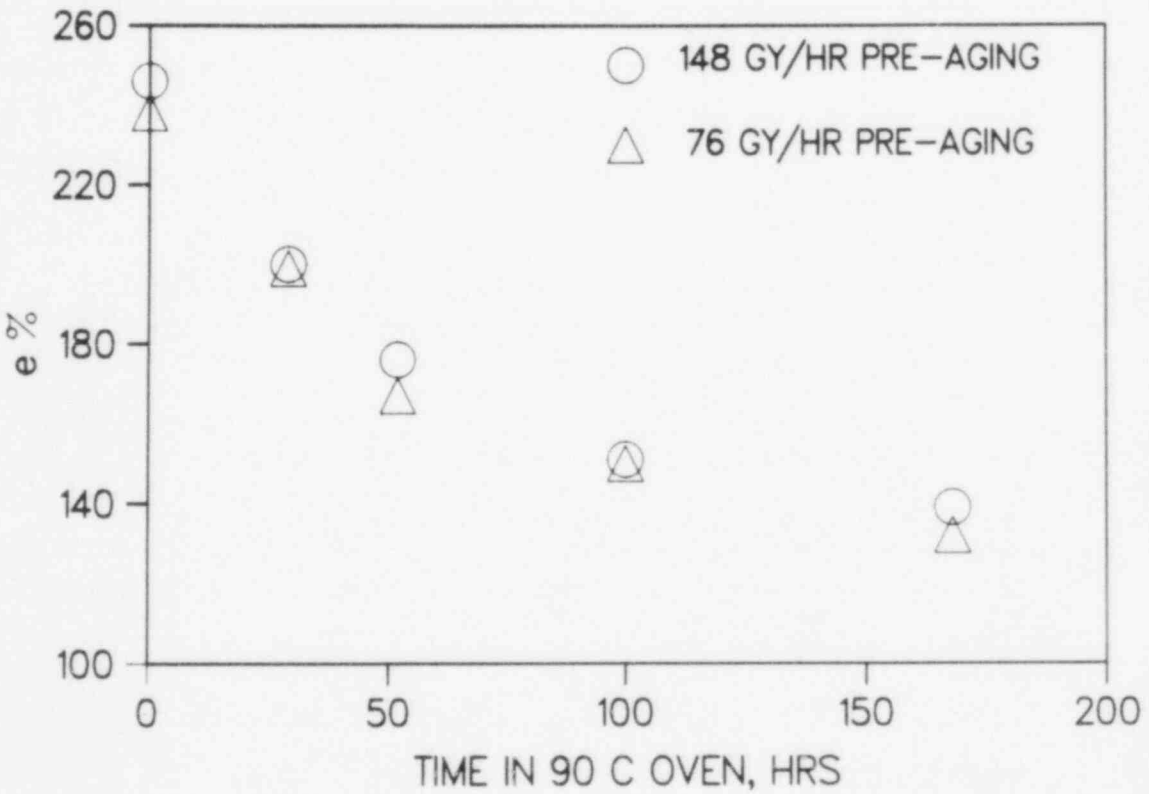

Figure 4. Comparison of the elongation vs. time responses in a 90°C oven for PVC samples previously radiation aged to the same total dose at 43°C and two different dose rates.

We can now kinetically analyze the reaction scheme shown in Equations (2)-(9). For convenience we will include RH and O_2 in the rate constants; i.e., $k_1 = k_1'(O_2)$, $k_2 = k_2'(RH)$, $k_5 = k_5'(RH)$, and $k_6 = k_6'(RH)$. If we assume that the degradation products, P, responsible for changing the macroscopic degradation variable being monitored (e.g., ultimate tensile elongation) will be some linear combination of the products generated by the kinetics, i.e.,

$$P = a\,P_{term} + b\,P_{int} \tag{10}$$

then kinetic analysis (the details are in the Appendix) yields:

$$P = \left(\frac{ak_7 + bk_3}{k_7}\right) k_I \frac{I}{k_4} \left\{ \frac{R}{R-1}\, k_4 t + \frac{R}{(R-1)^2}\left[\exp\left(\frac{(1-R)}{R}\right)k_4 t\right) - 1\right] \right\} \tag{11}$$

where t is the time, and

$$R = \frac{k_7}{2k_2} \quad . \tag{12}$$

Equation (11) directly predicts radiation dose-rate effects at constant temperature due to the slow breakdown of hydroperoxides. By choosing values for k_4, R, and the dose required for a given amount of damage to occur at high dose rates (where ROOH breakdown is not important), we calculate the product concentration corresponding to this dose. We can lower I and find the time required, t_i, at this lower dose rate to generate the same amount of product (and therefore the same material damage). The dose required would then be It_i. In this manner, isoproduct curves giving dose to equivalent damage (DED) versus dose rate can be generated. Examples of such theoretical dose-rate curves are shown in Figure 5 for values of R between 0.1 and 2. Since changes in the value of k_4 cause horizontal shifts in the curves but do not affect the shapes of the curves, the abscissa can be plotted universally as the dose rate divided by the ROOH breakdown constant. At high dose rates, the curves approach horizontal behavior (no dose-rate effects). For the theoretical curves shown in Figure 5, 300 kGy is arbitrarily picked for the DED in this region.

Model predictions concerning dose-rate effects are strongly dependent on the value of R. When R is greater than 1, less

than one ROOH is formed for every ROOH that breaks down; this implies that the ROOH concentration will tend towards a limiting value with time (Case I). As shown in Figure 5, this yields dose-rate effects which eventually disappear as the dose rate is lowered. For R = 1 (one ROOH formed for each ROOH that breaks down), the slope of the dose-rate effect curve at low dose rates approaches 0.5. When R is less than unity (more than one ROOH formed for each one that breaks down), dose-rate effects are predicted to continue increasing as the dose rate is lowered (Case II), with the slope eventually approaching 1.0.

The effect of changing the DED (i.e., looking at varying amounts of material degradation) under constant temperature conditions is theoretically predicted to be quite different for Case I and Case II behaviors. Figures 6 and 7 show theoretical curves for R = 1.25 and R = 0.5, respectively, using high dose-rate plateau

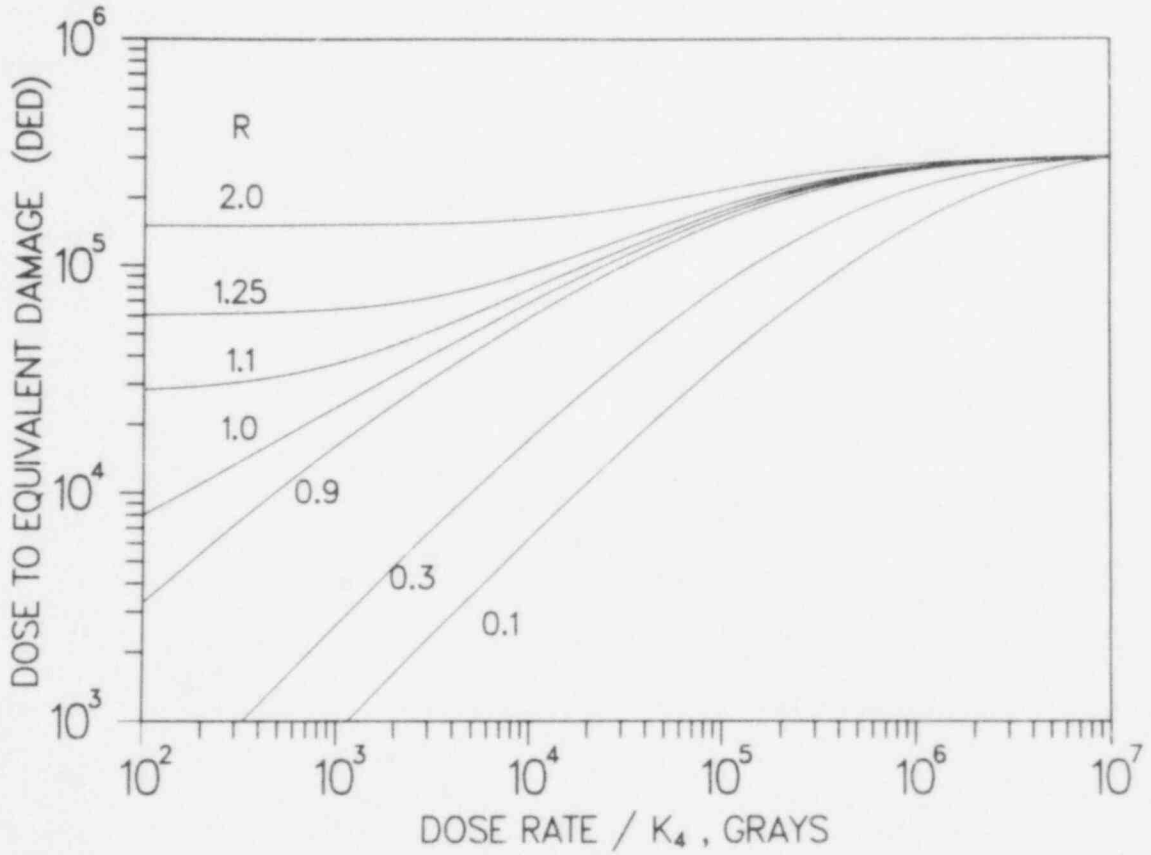

Figure 5. Theoretical model predictions for the relationship between the dose to equivalent damage (DED), and the dose rate divided by the rate constant for hydroperoxide breakdown. R is a positive constant which depends upon termination and propagation rate constants.

values for the DED of 50, 150, and 450 kGy. For both examples, increasing the DED by a factor of X causes the simultaneous horizontal and vertical shifting of the dose-rate effect curve by the factor X. In other words, for a constant value of R, one universal curve of constant shape represents the dose-rate behavior regardless of the amount of degradation. The horizontal location of this curve determines the value for the ROOH breakdown rate constant; the dose required for a given amount of degradation in the absence of ROOH breakdown (the high dose-rate plateau) is obtained from the vertical positioning of the curve. As the dose rate is lowered under constant temperature conditions (k_4 = constant), the model predicts earlier onset of dose-rate effects for higher levels of degradation. When R > 1 (Figure 6), this leads to a small compression of the vertical results in the region where the dose-rate effects are largest and an earlier establishment of ROOH steady state conditions (leveling out at low dose rates) at the higher levels of degradation. When R < 1, the theoretical results are much more interesting (Figure 7), since they predict quite different shapes for the dose-rate data as the DED changes. This is due to horizontal and vertical shifts of a universal R = 0.5 curve as pointed out above. In other words, the different DED's represent different sections of one universal curve.

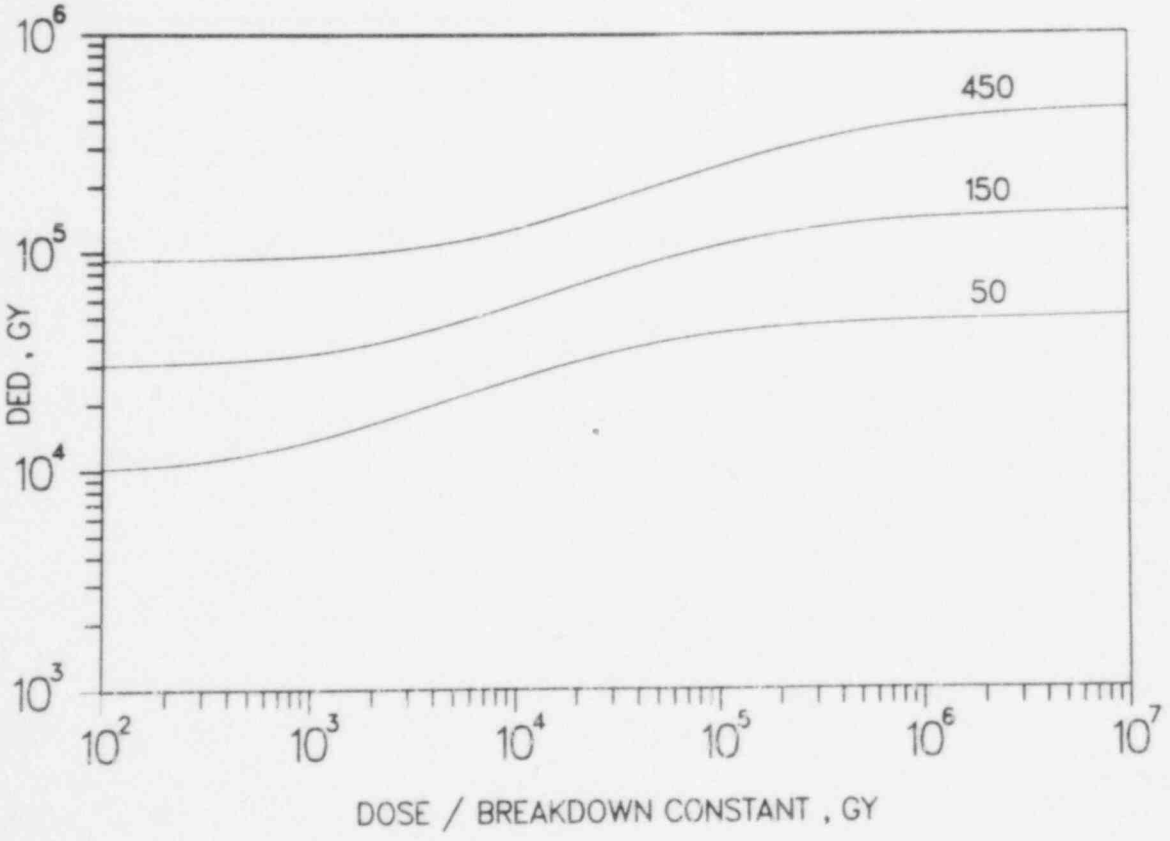

Figure 6. Variation of the theoretical model curves for R = 1.25 (Case I behavior) as the Dose to Equivalent Damage is varied.

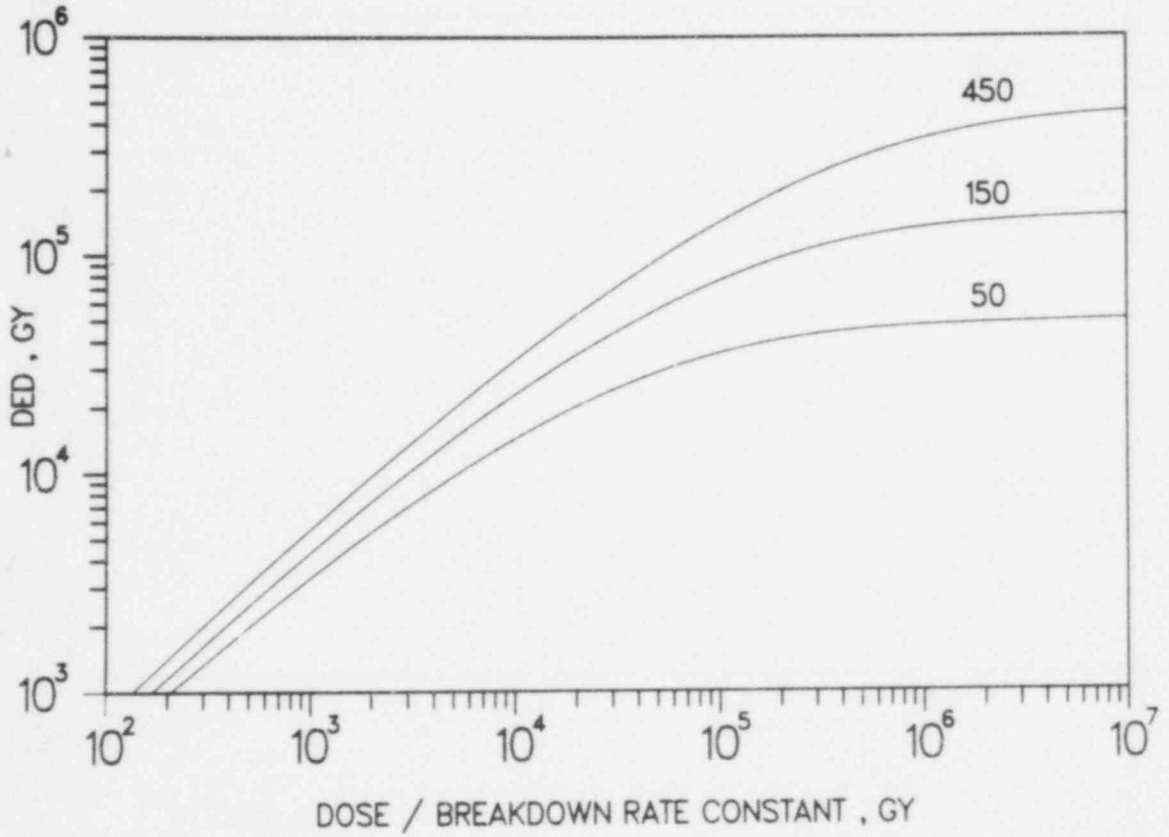

Figure 7. Variation of the theoretical model curves for R = 0.5 (Case II behavior) as the Dose to Equivalent Damage is varied.

Development and Use of Time-Temperature Dose-Rate Shift Procedure

In order to apply the theoretical results to the homogeneous combined environment data for PVC in Figure 2, we first note that the experimental data extends over approximately one-and-a-half orders of magnitude, an insufficient range to allow direct fits to the theoretical curves. This is normally the case since data extending over approximately 4 orders of magnitude in dose rate is required to typically characterize the S-shaped curves corresponding to Case I theoretical behavior. Sequential aging experiments coupled with sequential theoretical analysis sometimes allow us to circumvent this problem by developing a time-temperature dose-rate shift procedure. Using this procedure, the higher temperature results are shifted to a lower reference temperature, thereby extending the lower temperature results to lower dose rates. For a sequential exposure comprising a low-temperature radiation exposure followed by air-

oven aging, we will let $(ROOH)_0$ represent the ROOH concentration which has built up after the radiation aging. During the oven aging portion of the sequence at a temperature, T, the kinetic mechanism is identical to Equations (3)-(9). In other words, the radiation initiation step is eliminated; in its place, the initiation during oven exposure comes exclusively from breakdown of the $(ROOH)_0$ which was formed during the radiation aging part of the sequence. Solving for the sequential product versus time yields:

$$P_s^T = \frac{2(ak_7^T + bk_3^T)}{k_7^T - 2k_2^T} (ROOH)_0 \left\{1 - \exp\left|\frac{(1 - R^T)}{R^T} k_4^T t\right|\right\}. \quad (13)$$

Here, the superscript T on each parameter denotes the value of that parameter at the oven-aging temperature, T. P_s^T represents the degradation product generated during the oven exposure at temperature, T, and

$$R^T = \frac{k_7^T}{2k_2^T} . \quad (14)$$

When $R^T > 1$, less than one ROOH will be formed for every ROOH that breaks down, implying that the original concentration of $(ROOH)_0$ will eventually be exhausted. Thus P_s^T will approach the limiting value

$$P_s^T = \frac{2(ak_7^T + bk_3^T)}{k_7^T - 2k_2^T} (ROOH)_0 . \quad (15)$$

A material parameter which is dependent on the amount of degradation product generated would therefore be expected to start changing when first placed in the oven, but eventually level out at long times. Such behavior is observed for the PVC material. Figure 8 shows thermal aging data at three different sequential aging temperatures for PVC samples preirradiated under identical conditions. The results have been time-temperature shifted to 70°C as a reference temperature using an activation energy which gives the best superposition of the data, 23 $\pm$3 kcal/mole. The leveling out of the results implies that $R^T > 1$. In addition, since $(ROOH)_0$is identical for the three sets of oven-aged samples and the amount of drop to the degradation parameter plateau is independent of temperature, Equation (15) shows that $2(ak_7^T + bk_3^T)/(k_7^T - 2k_2^T)$ must have little dependence on

temperature. Although it is possible that the temperature dependencies of k_2, k_3, and k_7 could be quite different and still accidentally yield a negligible temperature dependence for the above expression, it is much more reasonable to assume that the temperature independence implies that the activation energies for the three rate constants are similar. This implies that R^T is insensitive to temperature and therefore, from Equation (13), that the estimated activation energy used to time-temperature superpose the data must represent the activation energy for k_4.

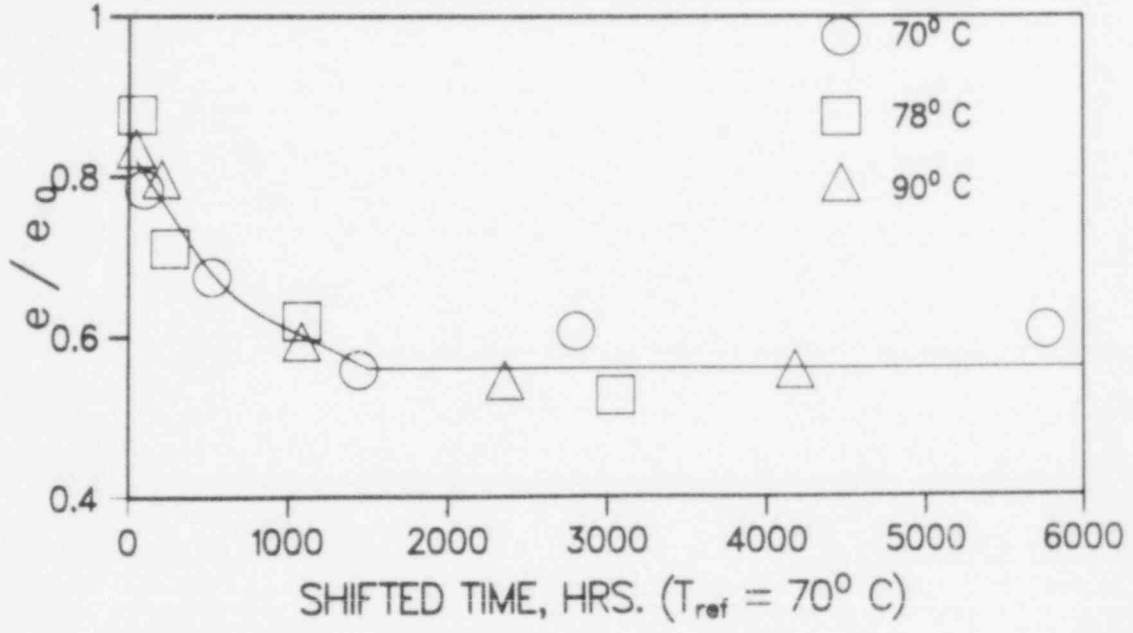

Figure 8. Time-temperature superposition of the thermal portion of sequential radiation followed by thermal aging experiments on PVC. The shifted time represents the shift factor a_T [defined in Eq. (18)] times the oven aging time, t, at the temperature, T. T_{ref} = 343°K.

Further support for the conclusion that the peroxide activity in preirradiated samples decreases with time during the oven exposure in sequential experiments has been obtained. Thermally-induced chemiluminescence in organic materials is believed to be primarily associated with peroxide decomposition reactions. Luminescence values measured for the initial light output from three PVC samples heated at 150°C (in counts per second above background levels of 100 cps) are given below.

1. For unirradiated material: 150 cps.

2. For material irradiated at ambient temperature and 440 Gy/h to a dose of 8.8×10^4 Gy: 1450 cps.

3. For material irradiated identically as for Case 2 above, but then subjected to 80°C for 83 days prior to luminescence measurements: 400 cps.

The decrease in chemiluminescence after heat aging is clearly consistent with having an R^T greater than one.

We now use Equation (11) (the degradation product result appropriate to simultaneous radiation-thermal aging conditions) to develop a time-temperature dose-rate shifting procedure for the simultaneous data. The sequential results imply that the temperature dependence of Equation (11) is due predominantly to the temperature dependence of k_4. This experimental conclusion is consistent with expectation, since k_4 should have a significantly higher E_a than the other rate constants involved. We define a temperature shift factor for shifting data from a temperature, T_1, to a reference temperature, T_{ref} as

$$a_T = \exp\left[\frac{23 \text{ kcal/mole}}{R_g}\left(\frac{1}{T_{ref}} - \frac{1}{T_1}\right)\right] \qquad (16)$$

where R_g is the universal gas constant. Suppose we wanted to extend the hypothetical dose-rate data at T_{ref} in Figure 9 to lower dose rates by utilizing a higher temperature result at point p_1. Since only k_4 and I depend on dose rate and temperature, Equation (11) gives

$$P = P(I, k_4, t) \quad . \qquad (17)$$

The degradation product at point P_1 depends on I_1 (the dose rate) $k_4^{T_1}$ (the hydroperoxide breakdown constant at T_1), t_1 (the time) and a number of constants. With

$$t_1 = (DED)_1/I_1$$

$$P_1 = P\left[I_1, k_4^{T_1}, (DED)_1/I_1\right] \quad . \qquad (18)$$

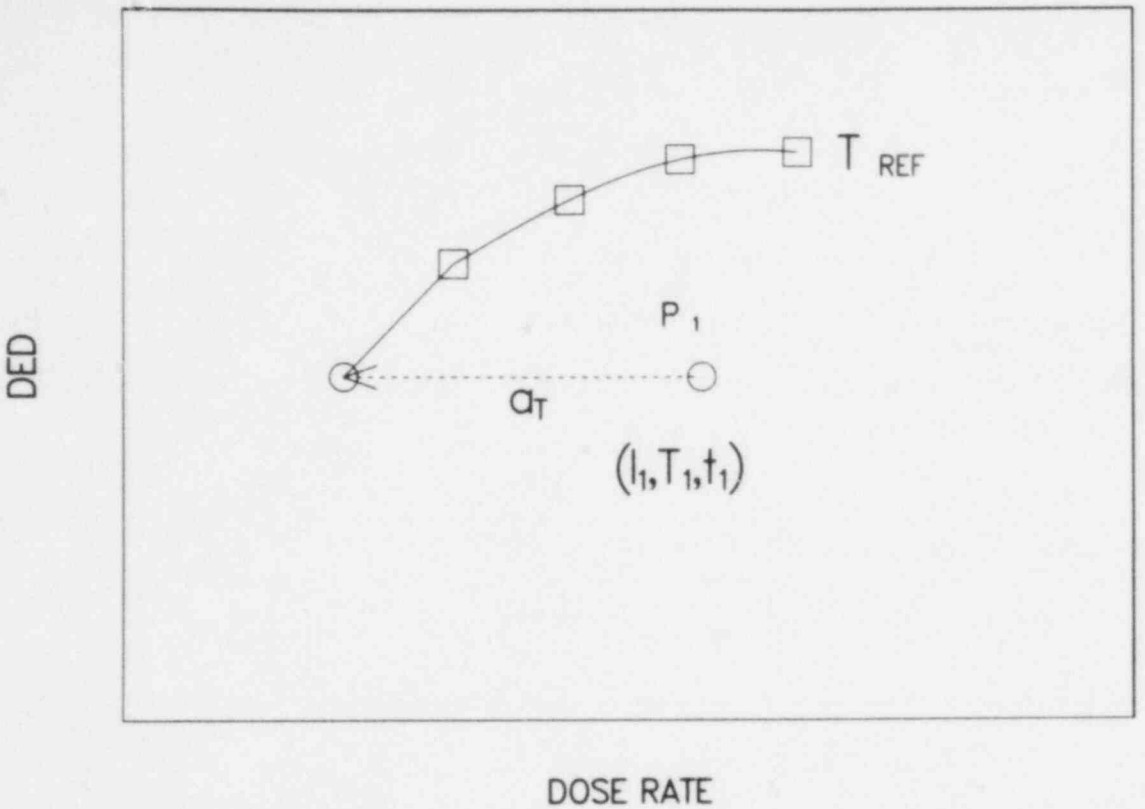

Figure 9. Hypothetical data showing schematically how a higher temperature data point, P_1, is time-temperature dose-rate shifted so that lower temperature data at T_{ref} can be extended to lower dose rate conditions.

We can change $k_4^{T_1}$ to the desired reference temperature by dividing by a_T. If we keep $(DED)_1$ constant and divide I_1 by a_T, we obtain

$$P\left[\frac{I_1}{a_T}, \frac{k_4^{T_1}}{a_T}, \frac{(DED)_1}{(I_1/a_T)}\right] \qquad (19)$$

which represents conditions at the reference temperature which are exactly equivalent (same product, same dose to failure), to point p_1. We therefore have a method for time-temperature dose-rate shifting of multistress data. In practice, this shift procedure is accomplished by a horizontal shift (DED constant) by a factor a_T on the dose-rate axis as shown in Figure 9.

Most shift procedures, such as time-temperature superposition, have one or more adjustable parameters (e.g., Arrhenius activation energy, WLF constants) which are empirically derived from the functional form of the shift parameters that give the best superposition of the shifted data. Even though we are treating the more complicated multistress cases, our shift procedure has no adjustable parameters; the functional form of the simultaneous shift parameter is obtained from separate sequential experiments.

Using the 23 kcal/mole activation energy for k_4 obtained from the sequential experiments on PVC, we use the above shifting procedure to shift the homogeneous and the borderline (nearly homogeneous) data of Figure 2 to a reference temperature of 43°C. The results are shown in the upper curve of Figure 10; the superposition for data covering a temperature range from 43°C to 110°C offers excellent evidence for the assumptions underlying the shift procedure. By utilizing the shift procedure, we have extended the 43°C data down to an equivalent dose rate of approximately 0.1 Gy/h, which is representative of ambient nuclear power plant aging conditions which we are trying to model. The resulting 43°C dose-rate curve is S-shaped with apparent plateau regions (no dose-rate effects) at high and low dose rates. This is identical to the theoretical model predictions (Figure 5) for Case I behavior ($R > 1$). The shape of the experimental curve can best be fit with an $R = 1.25$, which is shown by the solid theoretical curve of Figure 10 that was derived using this value. This value of R implies $k_7 = 2.5\ k_2$; the similar magnitude for these rate constants is consistent with the similar activation energies inferred earlier from the sequential results. The horizontal positioning of the theoretical curve allows us to obtain

$$k_4 = (5.6 \pm 1) \times 10^{-4} h^{-1} \text{ at } 43°C \quad .$$

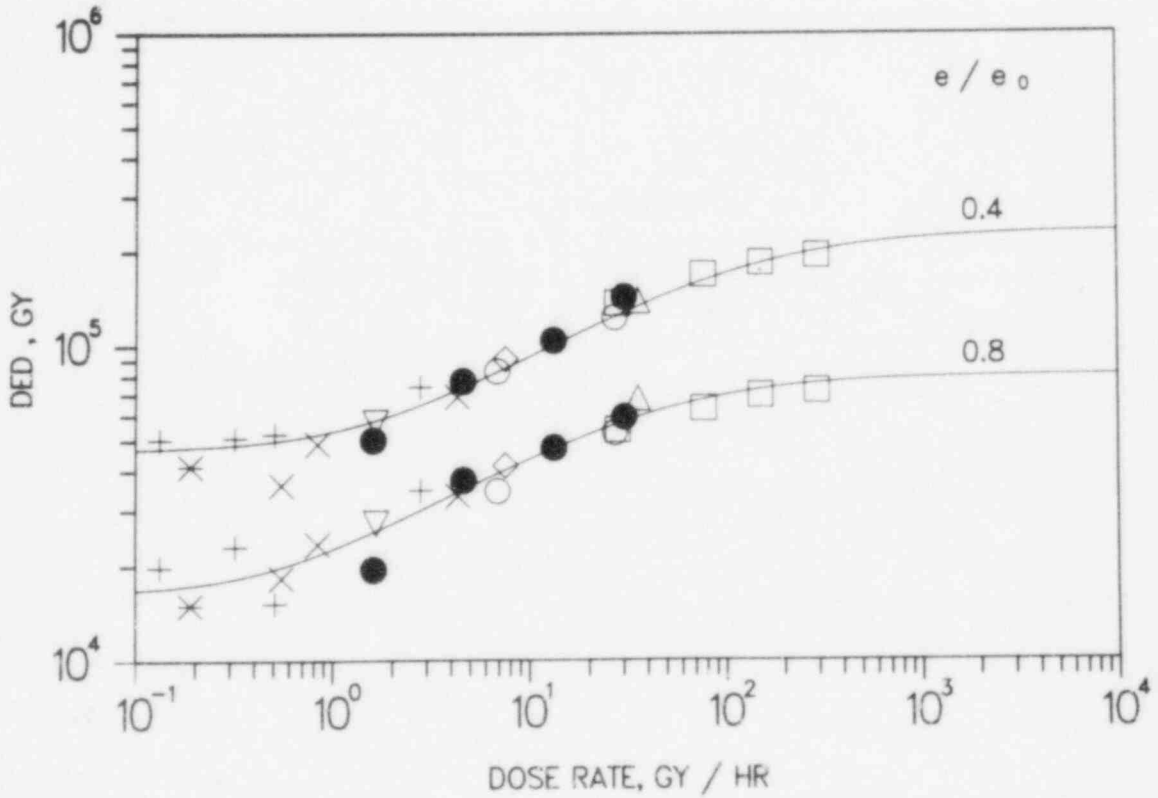

Figure 10. Upper data represents the homogeneous PVC data of Figure 2 ($e/e_0 = 0.4$) shifted to a reference temperature of 43°C. Symbols have same meaning as in Figure 2. Solid curve represents theoretical fit to the shifted data ($R = 1.25$, $k_4 = 5.6 \times 10^{-4} h^{-1}$). Lower data and curve are for $e/e_0 = 0.8$ data.

The vertical positioning predicts that in the absence of ROOH breakdown, a dose of 2.3×10^5 Gy would be required to cause e/e_o to drop to 0.4. This corresponds to degradation product generation of 2.3×10^5 C_k, where

$$C_k = \frac{(ak_7 + bk_3)\, k_I}{k_7} \quad . \tag{20}$$

As the dose rate is lowered, the product generated remains constant (for a constant drop in elongation) but the dose required drops due to the increasing importance of the ROOH breakdown mechanism. Although the experimental data has only been extended to a dose rate of 0.1 Gy/h, the model fit allows us to make predictions at still lower dose rates. Also note that the extremely small value of k_4 derived from the curve is consistent with the very long times expected for hydroperoxide breakdown at low temperatures.

The values of k_4 and R derived at $e/e_o = 0.4$ should be independent of damage and we verify this by showing experimental shifted results at $e/e_o = 0.8$ (lower curve of Fig. 10) and 0.6 in Figure 11, together with theoretical curves generated using identical values for k_4 and R. The amount of degradation product necessary to drop the elongation to 80 percent and 60 percent of initial is 8×10^4 C_k and 1.52×10^5 C_k, respectively. The same theoretical parameters give a reasonable fit to the shifted data for the tensile strength of this material as shown in Figure 12. The reason for choosing 26 percent drop in tensile strength for this figure will become clear below. Figure 13 plots the degradation product obtained from the theoretical fits in Figures 10 and 11 versus the corresponding changes in elongation. This transfer curve, which allows us to connect the unknown degradation product from the theoretical kinetics with the experimentally measured degradation variable, is approximately linear for this PVC material.

Comparison of Predicted and Experimental Sequential Exposures

To show the internal consistency of the results, we can use this transfer curve together with the derived kinetic parameters to quantitatively predict the mechanical degradation response for a sequential aging exposure. The radiation part of the experimental sequential exposure was carried out for 764 h at 45 Gy/h and 60°C, conditions chosen to assure completely homogeneous degradation. The ROOH concentration at the completion of the radiation exposure, and therefore the initial concentration for the subsequent oven aging part of the sequence, can be calculated to be

$$(\mathrm{ROOH})_o = \frac{k_I I}{2(R-1)k_4} \left\{ 1 - \exp\left(\frac{(1-R)}{R}\right) k_4 t \right\} \quad . \tag{21}$$

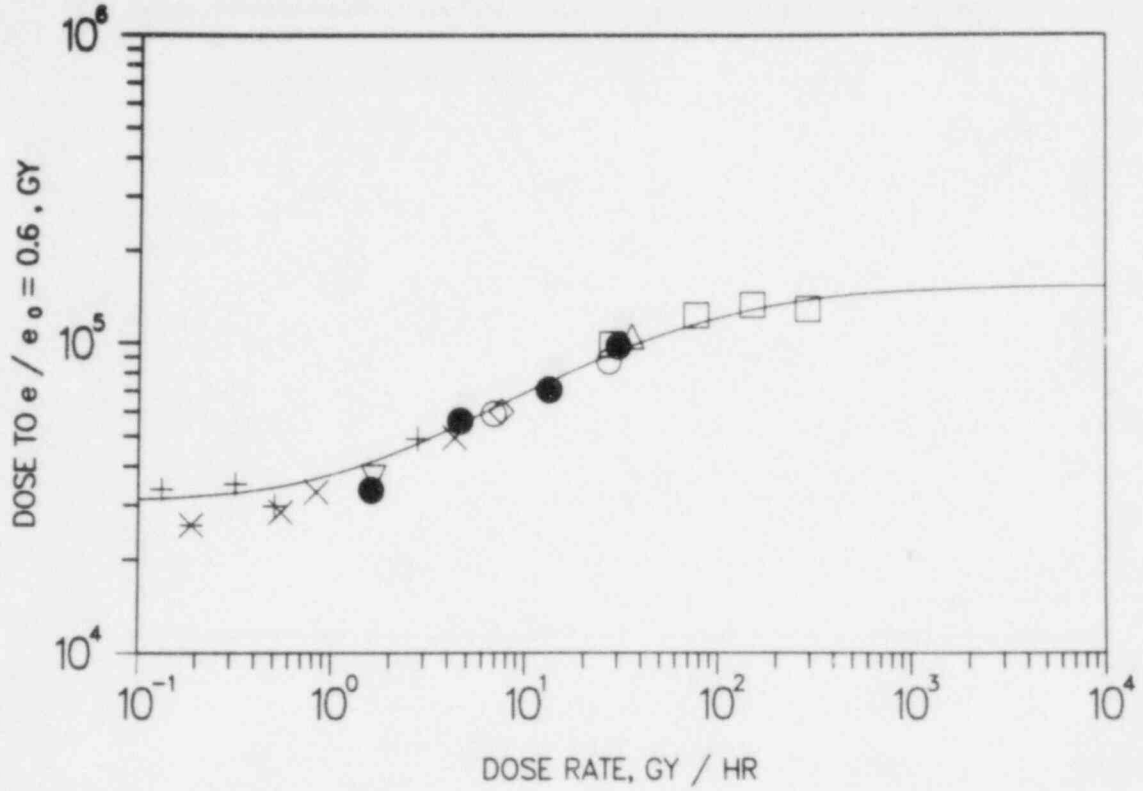

Figure 11. Homogeneous PVC elongation data for $e/e_o = 0.6$ shifted to a reference temperature of 43°C. Solid curve is theoretical fit using same values for R and k_4 as derived for Figure 10 data.

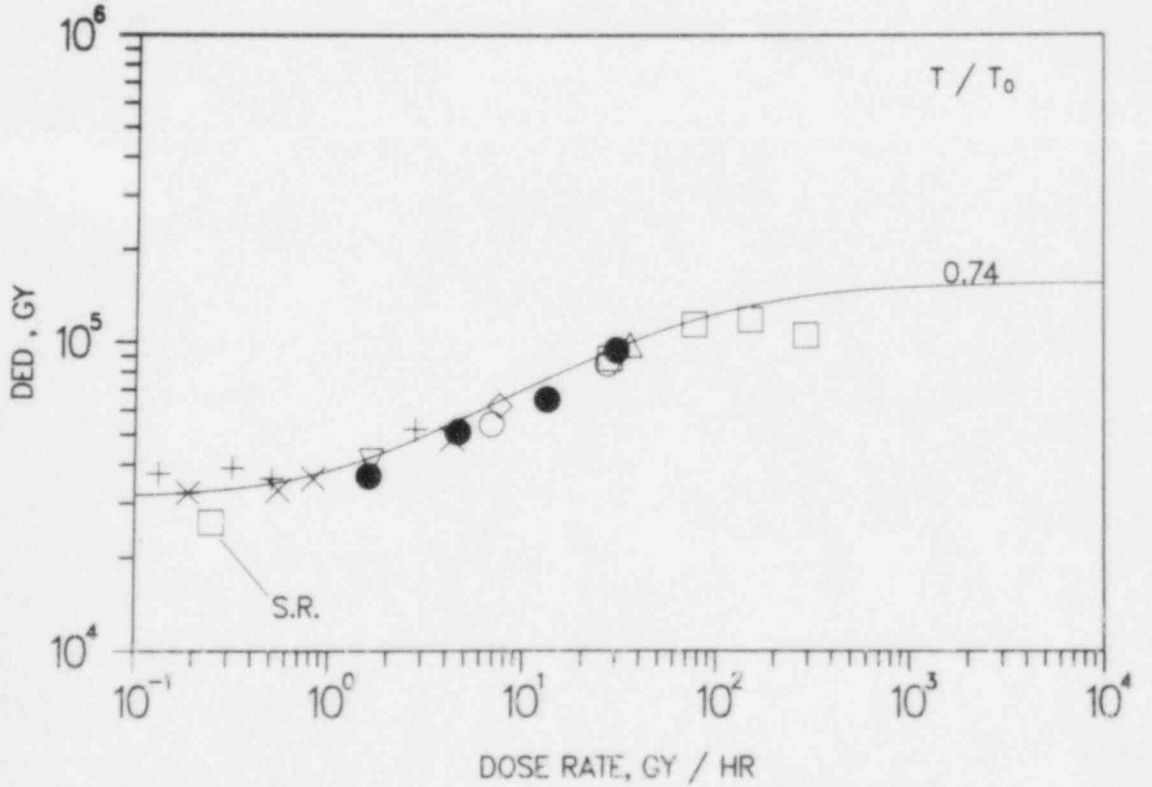

Figure 12. Homogeneous PVC tensile strength data shifted to a reference temperature of 43°C. Solid curve is theoretical fit using the same values of R and k_4 derived for Figure 10 data. S.R. denotes real-time data for material aged in the Savannah River reactor.

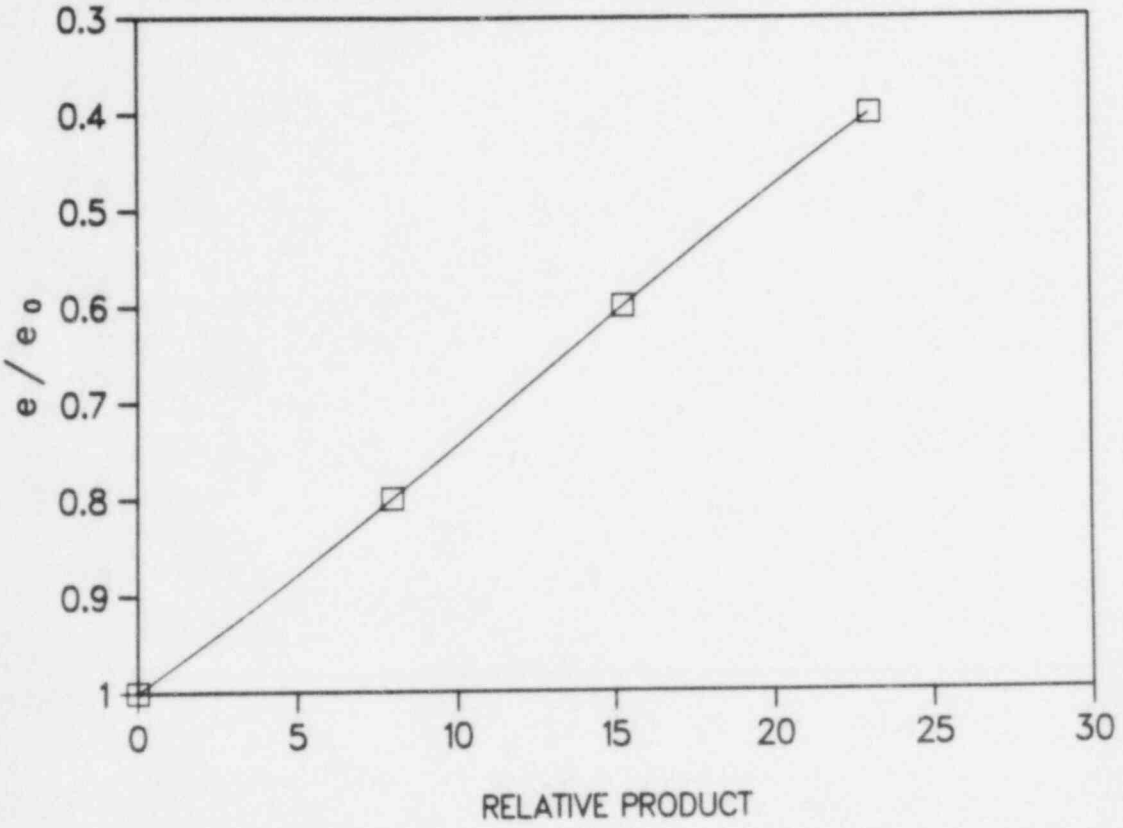

Figure 13. Relationship between the drop in tensile elongation of PVC and the relative amount of degradation product generated.

In this equation, k_4 is the ROOH breakdown rate constant at 60°C which is 3.63 x 10^{-3} h^{-1}, obtained from the value of k_4 in Figure 10 at 43°C and the shift factor using Equation (16). With t = 764 h, I = 45 Gy/h, and R = 1.25, we obtain

$$(ROOH)_0 = 1.06 \times 10^6 \, k_I \quad . \qquad (22)$$

Equation (11) can be used to show that the degradation product after the radiation exposure is given by

$$P = 6.65 \times 10^6 \, C_k$$

which corresponds from Figure 13 to $e/e_0 = 0.828$. The second part of the sequence, air-oven aging, was carried out at 80°C. Using Equations (13) and (22) leads to the following predicted results for the sequential degradation product versus time during 80°C oven exposure.

$$P_s = 1.06 \times 10^7 C_k \left| 1 - \exp\left(-5.21 \times 10^{-3} t\right) \right| . \qquad (23)$$

By adding these results to the predicted product occurring after the radiation exposure and using Figure 13 to transform the results to elongation values, we can theoretically predict the time dependence of the elongation during the oven exposure. The results, shown by the solid curve in Figure 14, are in excellent agreement with the experimental points. The theory not only quantitatively predicts the amount of drop to the plateau region, but also the exponential time constant for the drop.

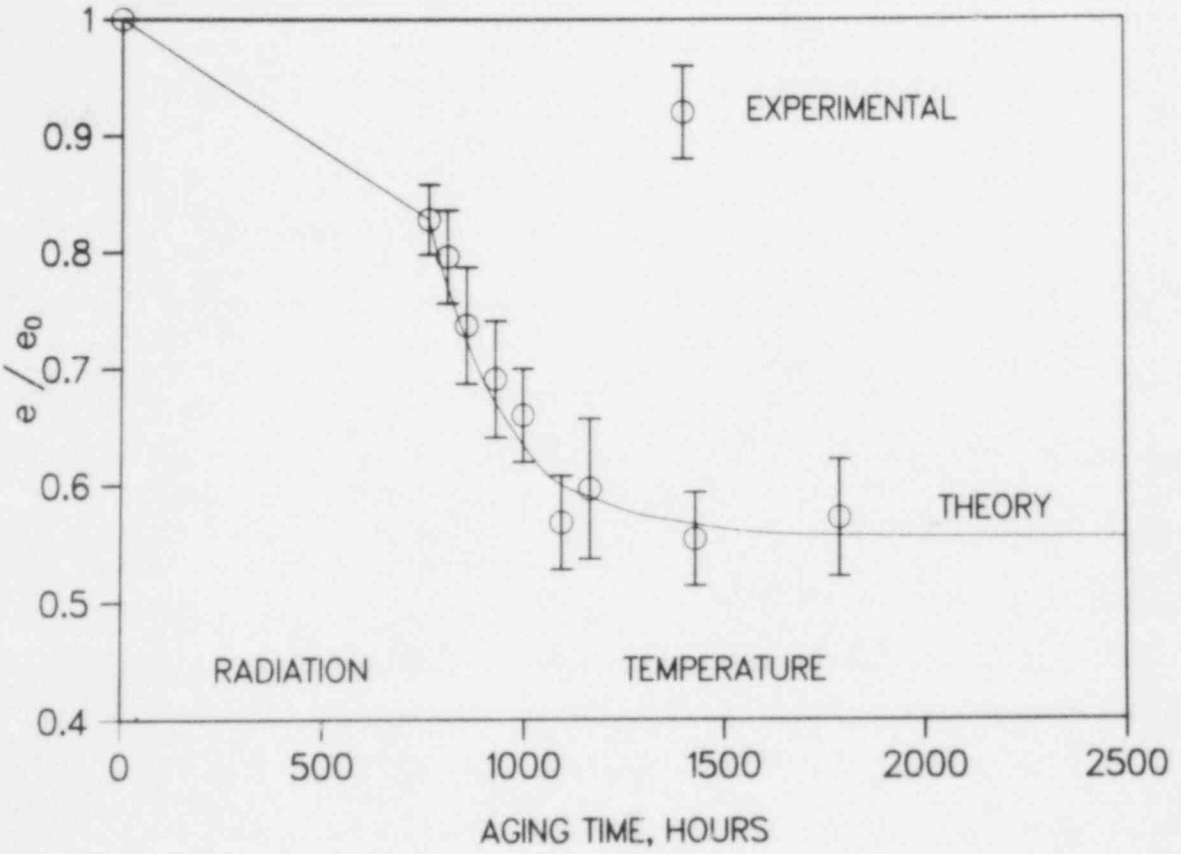

Figure 14. Relationship between tensile elongation and aging time for a sequential aging experiment. The experimental data (circles) is compared to the theoretical predictions (solid curve).

The value obtained for the rate constant k_4 compares favorably with the range or rate constants obtained for the breakdown of various hydroperoxides in solution.[25] The value is also consistent with data obtained for the breakdown constant of polymeric hydroperoxides at somewhat higher temperatures.[26,27]

Comparison of Extrapolated Model Predictions with Reactor-Aged Material

This same PVC material had been exposed as a cable jacket to 12 years of integrated reactor operation at the Savannah River Plant.[3,20] Figure 15 sketches the area of the plant from which the cable came. It entered the left-hand cable tray at the point marked B and exited through the concrete wall at point M. The highest mechanical degradation to the cable jacket occurred at the points marked D and F where the cable tray passed above heat-exchanger cooling lines. At these locations the PVC had reduced tensile elongation (e/e_o) and reduced tensile strength (T/T_o) values of 0.57 $\pm$ 0.03 and 0.74 $\pm$ 0.03, respectively. (The latter result is the reason we plotted 26 percent drops in tensile strengths in Figure 12.) Extensive environmental mapping at Savannah River indicated that the estimated conditions at points D and F averaged approximately 0.25 Gy/h and 43°C during the 12 years of reactor operation. Predictions based on the accelerated aging simulations fitted to the theoretical model are in excellent agreement with the real-time aging results. For e/e_o and T/T_o to reach 0.57 and 0.74, respectively at 0.25 Gy/h and 43°C, the model predicts 15 years and 14.5 years, respectively, versus 12 years for the real-time aged materials. The 12-year tensile strength point from the reactor is plotted in Figure 12, since it can be thought of as an experimental 43°C point.

Use of the Results to Predict and Simulate Aging

There are two main purposes of accelerated aging studies. First, one would like to be able to predict a material's or component's long-term behavior in an aging environment. Second, one would like to develop methodologies of aging the material to its equivalent lifetime in an accelerated time frame. This second goal becomes particularly important, for example, when lifetime aging must be simulated prior to a loss of-coolant-accident (LOCA) simulation. The resulting understanding of the dose-rate effects underlying the behavior of this PVC material together with the model parameters derived above allow us to achieve both goals. For instance, one can derive the time evolution of mechanical properties under chosen nuclear power plant aging conditions utilizing the 43°C (316°K) predictions in Figures 10-12 together with the known 23 kcal/mole activation energy for ROOH breakdown. If the assumed nuclear power plant aging conditions were 45°C (i.e., T_{ref} = 318°K) plus 0.1 Gy/h (10 rad/h), the curves in Figures 10-12 would need to be

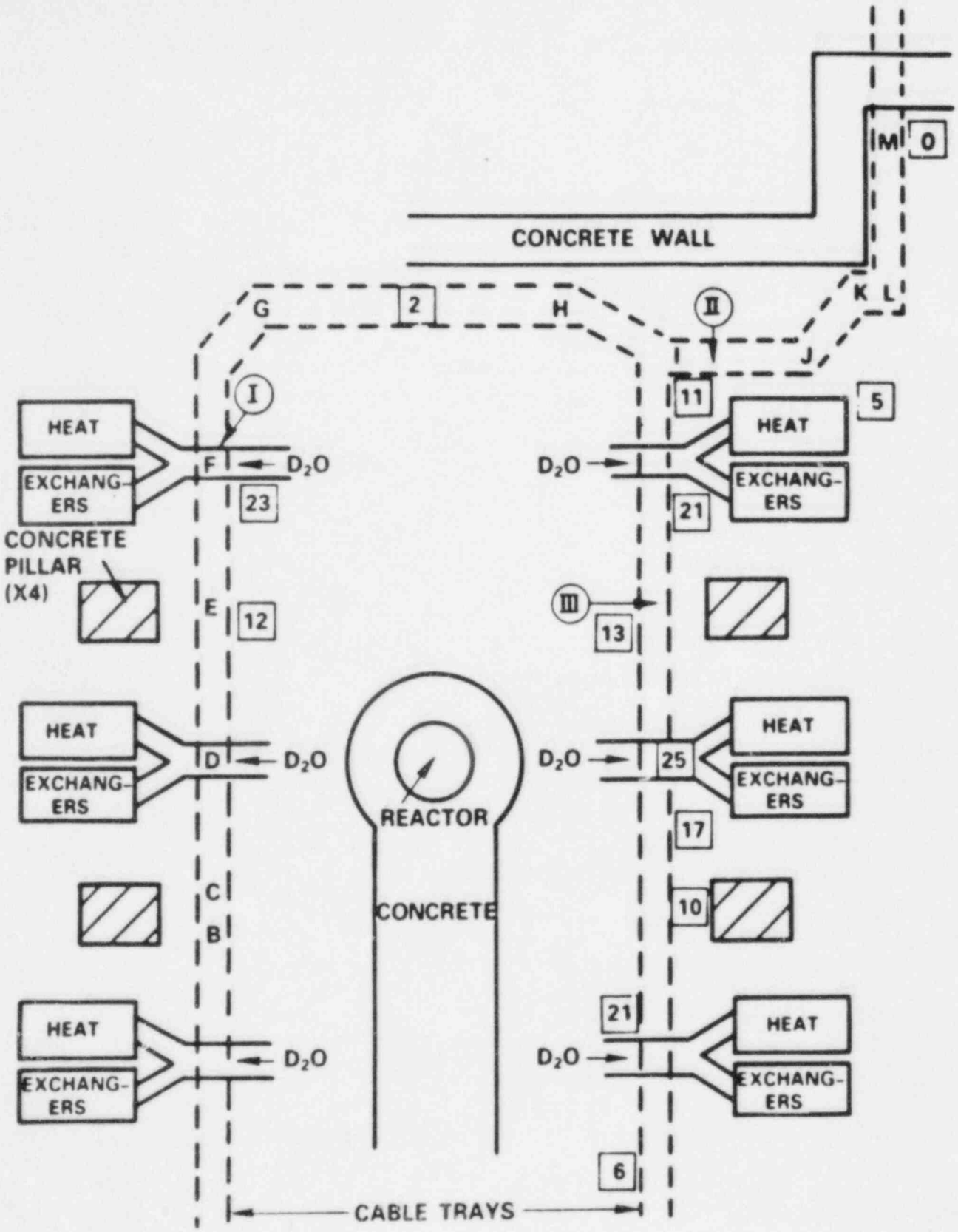

Figure 15. Schematic diagram of the containment building near the -6 m level of the Savannah River reactor.

shifted horizontally to higher dose rates by a factor of

a_T^{-1} where, from Eq. (16)

$$a_T^{-1} = \exp\left\{\frac{-23,000}{1.9865}\left(\frac{1}{318} - \frac{1}{316}\right)\right\} = 1.26$$

The resulting curves would then represent predicted 45°C dose-rate data, from which predictions at 0.1 Gy/h are easily obtained for e/e_o = 0.8, 0.6, 0.4 and T/T_o = 0.74. Using these results together with results from similar analyses at other degradation conditions (e.g. T/T_o = 0.9, 0.8, 0.7), we can than generate the predicted response of the mechanical properties for 45°C and 0.1 Gy/h aging conditions. The results, shown in Figure 16, indicate that this PVC material would still be in reasonable condition after 40 years under the above aging conditions.

If, on the other hand, we were interested in simulating 40 years at 45°C plus 0.1 Gy/h using accelerated conditions, the shift procedure described above and shown schematically in Figure 9 allows us to choose the proper conditions. For instance, at 110°C (i.e., T_{ref} = 383K)

$$a_T^{-1} = \exp\left\{\frac{-23,000}{1.9865}\left(\frac{1}{383} - \frac{1}{318}\right)\right\} = 483$$

Therefore damage equivalent to 40 yr at 0.1 Gy/h and 45°C would be predicted to occur at 110°C and a dose rate of 483 times 0.1 Gy/h or 48 Gy/h after $(483)^{-1}$ times 40 yr or 726 hr. Similar calculations at 100°C indicate that 1634 h at 100°C and 21 Gy/h would also be predicted to give equivalent damage.

Table II summarizes a number of accelerated conditions which are predicted by the present analysis to be equivalent to 40 yr at 45°C and 0.1 Gy/h. In choosing accelerated conditions, two constraints need to be mentioned. First the accelerated conditions must not result in heterogeneous degradation. For the conditions derived in Table II, this is clearly not a concern as can be seen from Figure 2. Second the accelerated temperature should not be much higher than the highest temperature used in generating the predicted results (110°C in the present case). This implies that the quickest simulation that could be done with reasonable confidence would take on the order of one month.

Table II
Aging Conditions Predicted to be Equivalent

Dose Rate Gy/h	T(°C)	Aging Time
0.1	45	40 years
3.7	80	9490 h
9.1	90	3840 h
21	100	1630 h
48	110	726 h

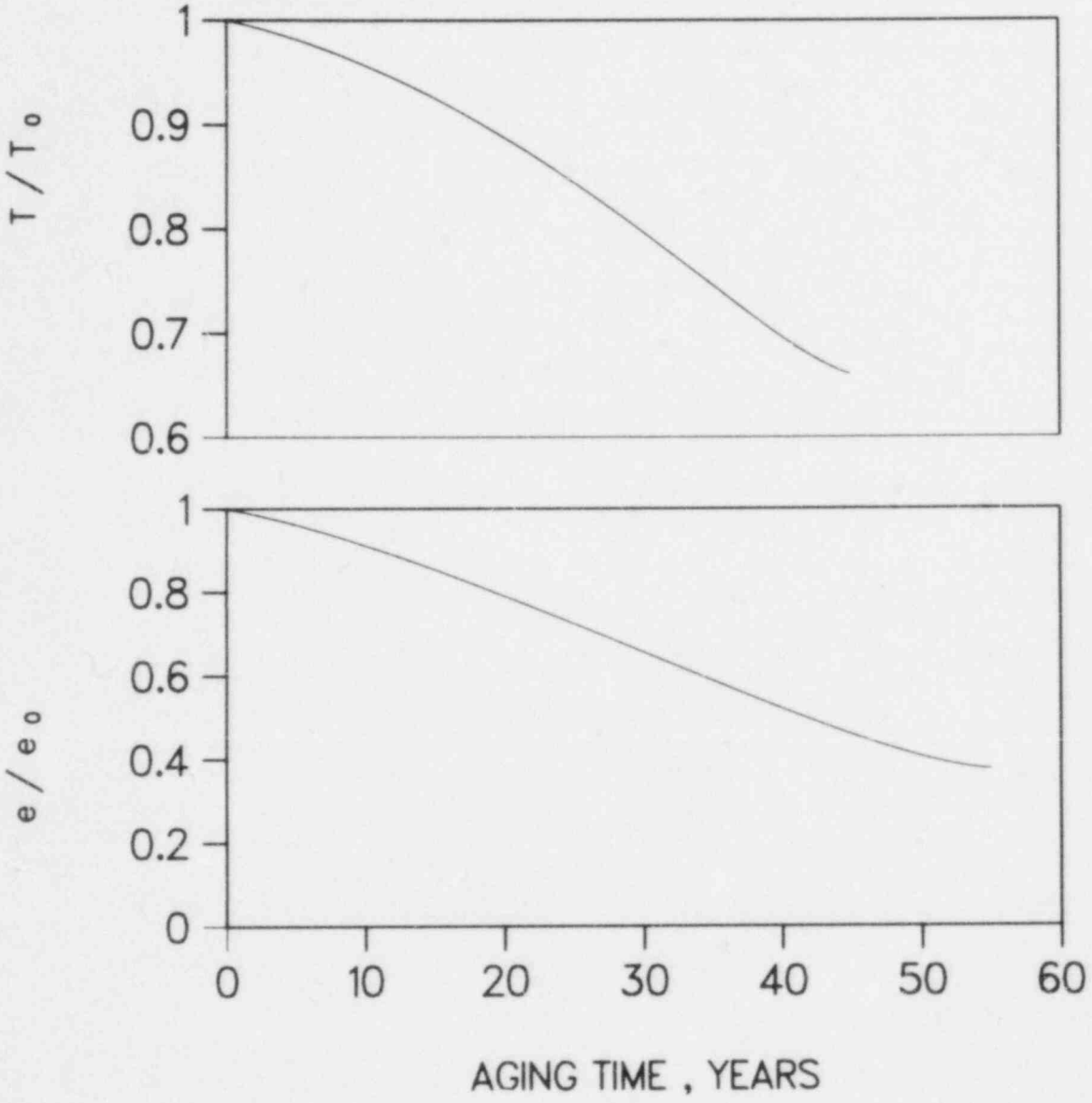

Figure 16. Mechanical property results predicted for PVC at 45°C plus 0.1 Gy/h.

It might seem remarkable that such a complicated material (two distinct dose-rate mechanisms) can be quantitatively understood with the results eventually used to choose accelerated aging conditions equivalent to 40-year real-time exposures. Unfor-

tunately, in addition to the model development, a very large number of experiments had to be run to separate the heterogeneous regions from the homogeneous regions and to derive the model parameters in the homogeneous region. The point to remember is that if you are trying to qualify a "complicated" material, the process can be complicated. For materials for which the hydroperoxide breakdown mechanism or other chemical dose-rate mechanisms are not important, the qualification process can become much easier since the equal damage-equal dose assumption may hold in the homogeneous region. In such a case, one would only have to insure (by means of profiling techniques) that the accelerated test was carried out at a dose rate sufficiently low that oxidation is essentially homogeneous. In other words, if dose-rate effects and synergistic effects for mildly elevated temperatures are not significant in the homogeneous region, accelerated predictions and simulations will become considerably simpler. The methods of this paper can be used to qualify complicated materials but they are perhaps more useful as a methodology/knowledge base which can be used to select and create better-formulated materials, in which chemical dose-rate effects are insignificant.

CONCLUSIONS

The degradation of PVC in combined radiation/thermal/air environments can be extremely complex due to at least two apparent dose-rate effect mechanisms: diffusion-limited oxidation and hydroperoxide-mediated degradation. Through the use of a recently-developed profiling technique (metallographic polishing), together with calculations based on oxygen consumption and permeation measurements, we can determine the radiation dose rate and temperature conditions under which diffusion-limited oxidation effects are present. This allows us to separate the homogeneous degradation regime (no diffusion effects) from the heterogeneous regime. In the homogeneous region, a theoretical kinetic model is derived which gives a general formalism for predicting radiation dose-rate effects. It is based on (1) a number of consensus reactions used for oxidation chemistry, (2) unimolecular termination kinetics (which are appropriate to cases of high radical-scavenger concentration and/or low dose rates), and (3) rate-determining hydroperoxide-mediated branching reactions. Evidence for these kinetics is presented for the PVC material. Theoretical analyses of sequential aging experiments allow a time-temperature dose-rate shift procedure to be developed and applied to this PVC material such that the theoretical model can be validated. Further validation occurs when model predictions for the PVC material are shown to be in excellent agreement with 12-year real-time aging results from a nuclear environment. The results can be used to predict material response in long-term aging environments and to choose accelerated aging conditions which create a material whose degradation is equivalent to that expected for a material aged to its lifetime conditions.

REFERENCES

1. K. T. Gillen and K. E. Mead, "Predicting Life Expectancy and Simulating Age of Complex Equipment Using Accelerated Aging Techniques," Sandia National Laboratories, SAND79-1561, NUREG/CR-1466, (January 1980).

2. K. T. Gillen and R. L. Clough, Radiat. Phys. Chem., 18, 667 (1981).

3. R. L. Clough and K. T. Gillen, J. Polym. Sci., Polym. Chem. Ed., 19, 2041 (1981).

4. R. L. Clough, K. T. Gillen, J. L. Campan, G. Gaussens, H. Schonbacher, T. Seguchi, H. Wilski and S. Machi, Nuclear Safety, 25, 238 (1984).

5. A. Charlesby, Proc. Roy. Soc., A215, 187 (1952).

6. D. Ballantine, G. Dienes, B. Manowitz, P. Ander and R. Mesrobian, J. Polym Sci., 13, 410 (1954).

7. L. St. Pierre and H. Dewhurst, J. Chem. Phys., 29, 241 (1958).

8. H. Matsuo and M. Dole, J. Phys. Chem., 63, 837 (1959).

9. H. Wilski, Kolloid Z.u.Z. Polymere, 251, 703 (1973).

10. F. Makhlis, Radiation Physics and Chemistry of Polymers, Wiley, NY (1975).

11. W. Schnabel, "Degradation by High Energy Radiation," in H.H.G. Jellinkek (ed.), Aspects of Degradation and Stabilization of Polymers, p. 172, Elsevier, Amsterdam (1978).

12. W. Schnabel, Polymer Degradation Principles and Practical Applications, p. 140, Hanser International, GDR (1981).

13. E. Niki, C. Decker and F. R. Mayo, J. Polym. Sci. P.C., 11, 2813 (1973).

14. C. Decker and F. R. Mayo, J. Polym. Sci. P.C., 11, 2847 (1973).

15. C. Decker, F. R. Mayo and H. Richardson, J. Polym. Sci., 11, 2879 (1973).

16. C. Decker, J. Appl. Polym. Sci., 20, 3321 (1976).

17. K. T. Gillen and R. L. Clough, Rad. Phys. and Chem., 22, 537 (1983).

18. K. Arakawa, T. Seguchi, U. Watanabe, N. Hayakawa, I. Kuriyama and S. Machi, J. Polym. Sci., Polym. Chem. Ed., 19, 2123 (1981).

19. T. Seguchi, K. Arakawa, N. Hayakawa and S. Machi, Radiat. Phys. Chem., 18, 671 (1981).

20. K. T. Gillen, R. L. Clough and L. H. Jones, "Investigation of Cable Deterioration in the Containment Building of the Savannah River Nuclear Reactor," Sandia National Laboratories, SAND81-2613, NUREG/CR-2877, (August 1982).

21. R. L. Clough, K. T. Gillen and C. A. Quintana, "Heterogeneous Oxidative Degradation in Irradiated Polymers," J. Polym. Sci. P.C., in press.

22. R. L. Clough and K. T. Gillen, Radiat. Phys. and Chem., 22, 527 (1983).

23. A. V. Cunliffe and A. Davis, Polym. Degr. and Stab., 4, 17 (1982).

24. E. A. Hegazy, T. Seguchi and S. Machi, J. Appl. Polym. Sci., 26, 2947 (1981).

25. R. Hiatt, in D. Swern (ed.) Organic Peroxides, Vol. II, Wiley, New York (1970), Ch. 1., p. 1.

26. J. Chien, J. Poly. Sci., A-1, 375 (1968).

27. J. Chien and H. Jabloner, J. Poly. Sci., A-1, 393 (1968).

APPENDIX

Derivation of Equation (11) from the Kinetics Given in Equations (2)-(9)

At the moderate to low dose rates and temperatures studied in the homogeneous region, we assume that k_4 is much smaller than the other rate constants, implying that the rate-determining steps are the initiation by radiation and the slow breakdown of hydroperoxides. This means that at any point in time, all the radical species can be estimated from steady state analysis. This leads to

$$(RO_2\cdot)_{ss} = \frac{k_I I + 2k_4(ROOH)}{k_7} \quad . \tag{A-1}$$

The time dependence of ROOH is then obtained by integrating

$$\frac{d(ROOH)}{dt} = k_2(RO_2\cdot) - k_4(ROOH) \tag{A-2}$$

with $RO_2\cdot$ substituted from above, yielding

$$(ROOH) = \frac{k_I I}{2k_4(R - 1)} \left\{ 1 - \exp\left[\frac{(1 - R)}{R} k_4 t \right] \right\} \tag{A-3}$$

where

$$R = \frac{k_7}{2k_2} \quad . \tag{A-4}$$

The free radical concentrations will follow that of ROOH through the steady state solutions. Since we are interested in determining the time dependence of degradation products, we note that

$$\frac{dP_{term}}{dt} = k_7(RO_2\cdot) = k_I I + 2k_4(ROOH) \quad . \tag{A-5}$$

Substituting the result for ROOH from above and integrating leads to

$$P_{term} = k_I \frac{I}{k_4} \left\{ \frac{R}{R - 1} k_4 t + \frac{R}{(R - 1)^2} \left[\exp\left(\frac{(1 - R)}{R} k_4 t \right) - 1 \right] \right\}. \quad \text{(A-6)}$$

It is easy to show that P_{int} is given by an expression identical to Equation (A-6) except for a multiplicative factor k_3/k_7. Assuming that the degradation products, P, responsible for changing the macroscopic degradation variable are some linear combination of these two products, i.e.,

$$P = a P_{term} + b P_{int} \quad \text{(A-7)}$$

leads to Equation (11).

DISTRIBUTION:

U.S. NRC Distribution Contractor
15700 Crabbs Branch Way
Rockville, MD 20850
375 copies for RV

Ansaldo Impianti
Centro Sperimentale del Boschetto
Corso F.M. Perrone, 118
16161 Genova
ITALY
Attn: C. Bozzolo

Ansaldo Impianti
Via Gabriele D'Annunzio, 113
16121 Genova
ITALY
Attn: S. Grifoni

ASEA-ATOM
Department KRD
Box 53
S-721 04
Vasteras
SWEDEN
Attn: A. Kjellberg

ASEA-ATOM
Department TQD
Box 53
S-721 04
Vasteras
SWEDEN
Attn: T. Granberg

ASEA KABEL AB
P.O. Box 42 108
S-126 12
Stockholm
SWEDEN
Attn: B. Dellby

Atomic Energy of Canada, Ltd.
Chalk River Nuclear Laboratories
Chalk River, Ontario K0J 1J0
CANADA
Attn: G. F. Lynch

Atomic Energy of Canada, Ltd.
1600 Dorchester Boulevard West
Montreal, Quebec H3H 1P9
CANADA
Attn: S. Nish

Atomic Energy Research Establishment
Building 47, Division M.D.D.
Harwell, Oxfordshire
OX11 ORA,
ENGLAND
Attn: S. G. Burnay

Bhabha Atomic Research Centre
Health Physics Division
BARC
Bombay-85
INDIA
Attn: S. K. Mehta

British Nuclear Fuels Ltd.
Springfields Works
Salwick, Preston
Lancs
ENGLAND
Attn: W. G. Cunliff, Bldg 334

Brown Boveri Reaktor GMBH
Postfach 5143
D-6800 Mannheim 1
WEST GERMANY
Attn: R. Schemmel

Bundesanstalt fur Materialprufung
Unter den Eichen 87
D-1000 Berlin 45
WEST GERMANY
Attn: K. Wundrich

CEA/CEN-FAR
Departement de Surete Nucleaire
Service d'Analyse Fonctionnelle
B.P. 6
92260 Fontenay-aux-Roses
FRANCE
Attn: M. Le Meur
J. Henry

CERN
Laboratorie 1
CH-1211 Geneve 23
SWITZERLAND
Attn: H. Schonbacher

Canada Wire and Cable Limited
Power & Control Products Division
22 Commercial Road
Toronto, Ontario
CANADA M4G 1Z4
Attn: Z. S. Paniri

Centro Elettrotecnico
Sperimentale Italiano
Research and Development
Via Rubattino 54
20134 Milan,
ITALY
Attn: Carlo Masetti

Commissariat a l'Energie Atomique
ORIS/LABRA
BP N° 21
91190 Gif-Sur-Yvette
FRANCE
Attn: G. Gaussens
J. Chenion
F. Carlin

Commissariat a l'Energie Atomique
CEN Cadarche DRE/STRE
BP N° 1
13115 Saint Paul Lez Durance
FRANCE
Attn: J. Campan

Conductores Monterrey, S. A.
P.O. Box 2039
Monterrey, N. L.
MEXICO
Attn: P. G. Murga

Electricite de France
Service Etudes et Projets Thermiques
et Nucleaires (S.E.P.T.E.N.)
Tour EDF GDF
Cedex N° 8
92080 Paris - La Defense
FRANCE
Attn: M. Herouard
M. Hermant

Electricite de France
Direction des Etudes et Recherches
1, Avenue du General de Gaulle
92141 CLAMART CEDEX
FRANCE
Attn: J. Roubault
L. Deschamps

Electricite de France
Direction des Etudes et Recherches
Les Renardieres
Boite Postale n° 1
77250 MORET SUR LORING
FRANCE
Attn: Ph. Roussarie
V. Deglon
J. Ribot

EURATOM
Commission of European Communities
C.E.C. J.R.C.
21020 Ispra (Varese)
ITALY
Attn: G. Mancini

FRAMATOME
Tour Fiat - Cedex 16
92084 Paris La Defense
FRANCE
Attn: G. Chauvin
E. Raimondo

Furukawa Electric Co., Ltd.
Hiratsuka Wire Works
1-9 Higashi Yawata - 5 Chome
Hiratsuka, Kanagawa Pref
JAPAN 254
Attn: E. Oda

Gesellschaft fur Reaktorsicherheit (GRS) mbH
Glockengasse 2
D-5000 Koln 1
WEST GERMANY
Attn: Library

Health & Safety Executive
Thames House North
Milbank
London SW1P 4QJ
ENGLAND
Attn: W. W. Ascroft-Hutton

ITT Cannon Electric Canada
Four Cannon Court
Whitby, Ontario L1N 5V8
CANADA
Attn: B. D. Vallillee

Imatran Voima Oy
Electrotechn. Department
P.O. Box 138
SF-00101 Helsinki 10
FINLAND
Attn: B. Regnell
K. Koskinen

Institute of Radiation Protection
Department of Reactor Safety
P.O. Box 268
00101 Helsinki 10
FINLAND
Attn: L. Reiman

Instituto de Desarrollo y Diseno
Ingar - Santa Fe
Avellaneda 3657
C.C. 34B
3000 Santa Fe
REPUBLICA ARGENTINA
Attn: N. Labath

Japan Atomic Energy Research Institute
Takasaki Radiation Chemistry
Research Establishment
Watanuki-machi
Takasaki, Gunma-ken
JAPAN
Attn: N. Tamura
K. Yoshida
T. Seguchi

Japan Atomic Energy Research Institute
Tokai-Mura
Naka-Gun
Ibaraki-Ken
319-11
JAPAN
Attn: Y. Koizumi

Japan Atomic Energy Research Institute
Osaka Laboratory for Radiation Chemistry
25-1 Mii-Minami machi,
Neyagawa-shi
Osaka 572
JAPAN
Attn: Y. Nakase

Kraftwerk Union AG
Department R361
Hammerbacherstrasse 12 + 14
D-8524 Erlangen
WEST GERMANY
Attn: I. Terry

Kraftwerk Union AG
Section R541
Postfach: 1240
D-8757 Karlstein
WEST GERMANY
Attn: W. Siegler

Kraftwerk Union AG
Hammerbacherstrasse 12 + 14
Postfach: 3220
D-8520 Erlangen
WEST GERMANY
Attn: W. Morell

Motor Columbus
Parkstrasse 27
CH-5401
Baden
SWITZERLAND
Attn: H. Fuchs

National Nuclear Corporation
Cambridge Road
Whetstone
Leicester LE8 3LH
ENGLAND
Attn: A. D. Hayward
J. V. Tindale

NOK AG Baden
Beznau Nuclear Power Plant
CH-5312 Doettingen
SWITZERLAND
Attn: O. Tatti

Norsk Kabelfabrik
3000 Drammen
NORWAY
Attn: C. T. Jacobsen

Nuclear Power Engineering Test Center
6-2, Toranomon, 3-Chome
Minato-ku
No. 2 Akiyana Building
Tokyo 105
JAPAN
Attn: S. Maeda

Ontario Hydro
700 University Avenue
Toronto, Ontario M5G 1X6
CANADA
Attn: R. Wong
B. Kukreti

Oy Stromberg Ab
Helsinki Works
Box 118
FI-00101 Helsinki 10
FINLAND
Attn: P. Paloniemi

Radiation Center of
Osaka Prefecture
Radiation Application-
Physics Division
Shinke-Cho, Sakai
Osaka, 593, JAPAN
Attn: S. Okamoto

Rappinl
ENEA-PEC
Via Arcoveggio 56/23
Bologna
ITALY
Attn: Ing. Ruggero

Rheinisch-Westfallscher
Technischer Uberwachunge-Vereln e.V.
Postfach 10 32 61
D-4300 Essen 1
WEST GERMANY
Attn: R. Sartori

Sydkraft
Southern Sweden Power Supply
21701 Malmo
SWEDEN
Attn: O. Grondalen

UKAEA
Materials Development Division
Building 47
AERE Harwell
OXON OX11 ORA
ENGLAND
Attn: D. C. Phillips

United Kingdom Atomic Energy Authority
Safety & Reliability Directorate
Wigshaw Lane
Culcheth
Warrington WA3 4NE
ENGLAND
Attn: M. A. H. G. Alderson

Waseda University
Department of Electrical Engineering
4-1 Ohkubo-3, Shinjuku-ku
Tokyo
JAPAN
Attn: K. Yahagi

1200 J. P. VanDeven er
1800 R. L. Schwoebel
1810 R. G. Kepler
1811 R. L. Clough
1812 L. A. Harrah
1812 K. T. Gillen
1813 J. G. Curro
1815 R. T. Johnson
2155 J. E. Gover
2155 O. M. Stuetzer
6041 E. E. Minor
6200 V. L. Dugan
6300 R. W. Lynch
6400 A. W. Snyder
6410 J. W. Hickman
6417 D. D. Carlson
6420 J. V. Walker
6440 D. A. Dahlgren
6442 W. A. Von Riesemann
6444 D. A. Dahlgren, Acting
6445 J. H. Linebarger
6445 P. R. Bennett
6445 L. D. Bustard
6445 E. H. Richards
6446 L. L. Bonzon (10)
6446 W. H. Buckalew
6446 J. W. Grossman
6446 D. B. Hente
6446 F. V. Thome
6446 F. J. Wyant
6447 D. L. Berry
6449 K. D. Bergeron
6450 J. A. Reuscher
8024 M. A. Pound
3141 C. M. Ostrander (5)
3151 W. L. Garner

NRC FORM 335 (2-84) NRCM 1102, 3201, 3202

U.S. NUCLEAR REGULATORY COMMISSION

BIBLIOGRAPHIC DATA SHEET

SEE INSTRUCTIONS ON THE REVERSE

1. REPORT NUMBER (Assigned by TIDC, add Vol. No., if any)
NUREG/CR-4008
SAND84-1948

2. TITLE AND SUBTITLE
GENERAL EXTRAPOLATION MODEL FOR AN IMPORTANT CHEMICAL DOSE-RATE EFFECT

3. LEAVE BLANK

4. DATE REPORT COMPLETED
MONTH: December YEAR: 1984

5. AUTHOR(S)
K. T. Gillen and R. L. Clough

6. DATE REPORT ISSUED
MONTH: December YEAR: 1984

7. PERFORMING ORGANIZATION NAME AND MAILING ADDRESS (Include Zip Code)
Sandia National Laboratories
P. O. Box 5800
Albuquerque, NM 87185

8. PROJECT/TASK/WORK UNIT NUMBER

9. FIN OR GRANT NUMBER
NRC FIN No. A-1051

10. SPONSORING ORGANIZATION NAME AND MAILING ADDRESS (Include Zip Code)
Electrical Engineering Instrumentation and Control Branch
Division of Engineering Technology
Office of Nuclear Regulatory Research
U.S. Nuclear Regulatory Commission
Washington, DC 20555

11a. TYPE OF REPORT

b. PERIOD COVERED (Inclusive dates)

12. SUPPLEMENTARY NOTES

13. ABSTRACT (200 words or less)

In order to extrapolate material accelerated aging data, methodologies must be developed based on sufficient understanding of the processes leading to material degradation. One of the most important mechanisms leading to chemical dose-rate effects in polymers involves the breakdown of intermediate hydroperoxide species. A general model for this mechanism is derived based on the underlying chemical steps. The results lead to a general formalism for understanding dose rate and sequential aging effects when hydroperoxide breakdown is important. We apply the model to combined radiation/temperature aging data for a PVC material and show that this data is consistent with the model and that model extrapolations are in excellent agreement with 12-year real-time aging results from an actual nuclear plant. This model and other techniques discussed in this report can aid in the selection of appropriate accelerated aging methods and can also be used to compare and select materials for use in safety-related components. This will result in increased assurance that equipment qualification procedures are adequate.

14. DOCUMENT ANALYSIS - a. KEYWORDS/DESCRIPTORS

b. IDENTIFIERS/OPEN-ENDED TERMS

15. AVAILABILITY STATEMENT
unlimited

16. SECURITY CLASSIFICATION
(This page) U
(This report) U

17. NUMBER OF PAGES
41

18. PRICE

Org.	Bldg.	Name	Rec'd by	Org.	Bldg.	Name	Rec'd by

120555078877 1 1AN1RV
US NRC
ADM-DIV OF TIDC
POLICY & PUB MGT BR-PDR NUREG
W-501
WASHINGTON DC 20555

Sandia National Laboratories